Biomedicine & Pharmacotherapy 160 (2023) 114350

Contents lists available at ScienceDirect

Biomedicine & Pharmacotherapy

journal homepage: www.elsevier.com/locate/biopha

Luteolin directly binds to KDM4C and attenuates ovarian cancer stemness via epigenetic suppression of PPP2CA/YAP axis

Yunzhe Li [a,1], Yunran Hu [b,c,1], Lingling Yang [d,1], Jingshu Liu [e], Chenxi Cui [d], Muyao Yang [a], Dongling Zou [f], Lei Zhou [g,h], Qi Zhou [f,*], Weihong Ge [b,c,**], Tingyuan Lang [f,i,***]

[a] College of Bioengineering, Chongqing University, Chongqing 400044, People's Republic of China
[b] Department of Pharmacy, Affiliated Drum Tower Hospital of Nanjing University Medical School, Nanjing 210008, Jiangsu Province, People's Republic of China
[c] School of Basic Medicine and Clinical Pharmacy, China Pharmaceutical University, Nanjing 210009, Affiliated Drum Tower Hospital of Nanjing University Medical School, Nanjing 210008, Jiangsu Province, People's Republic of China
[d] School of Medicine, Chongqing University, Chongqing 400044, People's Republic of China
[e] Obstetrics and Gynecology Department, The Second Affiliated Hospital of Chongqing Medical University, Chongqing 400010, People's Republic of China
[f] Department of Gynecologic Oncology, Chongqing University Cancer Hospital & Chongqing Cancer Institute & Chongqing Cancer Hospital, Chongqing 400030, People's Republic of China
[g] School of Optometry; Department of Applied Biology and Chemical Technology; Research Centre for SHARP Vision (RCSV), The Hong Kong Polytechnic University, Hong Kong
[h] Centre for Eye and Vision Research (CEVR), 17W Hong Kong Science Park, Hong Kong
[i] Reproductive Medicine Center, The First Affiliated Hospital of Chongqing Medical University, Chongqing 400042, People's Republic of China

ARTICLE INFO

Keywords:
Luteolin
Ovarian cancer
Cancer stem cells
KDM4C
PPP2CA
YAP

ABSTRACT

Long-term use of low-toxic natural products holds the promise for eradicating cancer stem cells. In this study, we report that luteolin, a natural flavonoid, attenuates the stemness of ovarian cancer stem cells (OCSCs) by directly binding to KDM4C and epigenetic suppression of PPP2CA/YAP axis. Ovarian cancer stem like cells (OCSLCs) isolated by suspension culture and CD133 + ALDH+ cell sorting was employed as OCSCs model. The maximal non-toxic dose of luteolin suppressed stemness properties, including sphere-forming capacity, the expression of OCSCs markers, sphere-initiating and tumor-initiating capacities, as well as the percentage of CD133 + ALDH+ cells of OCSLCs. Mechanistic study showed that luteolin directly binds to KDM4C, blocks KDM4C-induced histone demethylation of PPP2CA promoter, inhibits PPP2CA transcription and PPP2CA-mediated YAP dephosphorylation, thereby attenuating YAP activity and the stemness of OCSLCs. Furthermore, luteolin sensitized OCSLCs to traditional chemotherapeutic drugs in vitro and in vivo. In summary, our work revealed the direct target of luteolin and the underlying mechanism of the inhibitory effect of luteolin on the stemness of OCSCs. This finding thus suggests a novel therapeutic strategy for eradicating human OCSCs driven by KDM4C.

1. Introduction

Globally, more than 220,000 new cases of ovarian cancer (OC) are diagnosed each year, which leads to more than 140,000 cancer-specific deaths, making it the leading cause of cancer mortality; late diagnosis and development of therapeutic resistance contribute the high mortality rate [1]. The histologic subtypes of OC include epithelial cancers (serous, endometrioid, clear-cell and mucinous), small cell carcinoma, and non-epithelial cancers (germ-cell and sex cord stromal tumors); among them, high-grade serous carcinoma (HGSC) is the most common and the most serious subtype, which accounts for about 90% of the disease [2]. Cytoreductive surgery followed by platinum- and taxane-based

* Corresponding author.
** Corresponding author at: Department of Pharmacy, Affiliated Drum Tower Hospital of Nanjing University Medical School, Nanjing 210008, Jiangsu Province, People's Republic of China.
*** Corresponding author at: Department of Gynecologic Oncology, Chongqing University Cancer Hospital & Chongqing Cancer Institute & Chongqing Cancer Hospital, Chongqing 400030, People's Republic of China.
E-mail addresses: cqzl_zq@163.com (Q. Zhou), glg6221230@163.com (W. Ge), michaellang2009@163.com (T. Lang).
[1] These authors made equal contributions to this work.

https://doi.org/10.1016/j.biopha.2023.114350
Received 1 July 2022; Received in revised form 25 January 2023; Accepted 31 January 2023
Available online 16 February 2023

chemotherapy comprise the standard therapeutic strategy, while no remarkable increase in 10-year survival rate was achieved [3], which requires our improved understanding of the pathogenesis and therapeutic strategies of OC.

Cancer stem cells (CSCs) are a small subpopulation of cancer cells with stem-like properties in tumor tissue. CSCs keep distinct cellular characteristics associated with tumorigenesis, metastasis and therapeutic-response, which offers a reasonable explanation for relapse and therapeutic resistance of most types of cancers [4,5]. For example, 20% early-stage OC patients, whom R0 resection and complete response of primary therapy were achieved, will eventually relapse and resist to cytotoxic agents [6], indicating the fundamental roles of congenital superiority of ovarian cancer stem cells (OCSCs). Thus, CSCs have been recognized as principal targets for anticancer treatment. However, eradicating CSCs asks development of low-toxic anticancer drugs. Because of early metastasis and intrinsic resistance of CSCs, primary therapy is difficult to remove them. So, long-term administration of anticancer agents with lower toxicity and fewer side-effects for persistently suppressing of CSCs is urgently required.

Luteolin, a natural product, belongs to flavonoids [7]. Studies have shown the anticancer activities of this family members in multi-types of cancer cells [8]. Furthermore, luteolin possesses the ability to modify inflammatory environments, a well-known inducer of cancer transformation [9]. Most important, flavonoids are naturally occurred and exist widely in esculent plants and medicinal herbs, indicating its tolerance [7]. However, whether luteolin suppresses OCSCs has remained elusive.

In this study, we report that luteolin inhibits the stemness of OCSCs by directly binding to KDM4C and epigenetically suppressing KDM4C-mediated activation of PPP2CA/YAP axis. This finding provides a mechanical basis for development of luteolin as a novel anticancer drug for suppressing human OCSCs.

2. Materials and methods

2.1. Cell culture

Human OC cell line Caov-3 and HEK293T (Human embryonic kidney 293 T) cell line were obtained from American Type Culture Collection (ATCC, Manassas, VA, USA) and grown in Dulbecco's Modified Eagle's Medium (DMEM, 10566–016, Thermo Fisher, Waltham, MA, USA) containing 10% Fetal bovine serum (FBS, 26140079, Thermo Fisher, Waltham, MA, USA) and antibiotics (15240062, Thermo Fisher, Waltham, MA, USA) at 37 °C in 5% CO_2. The primary OC cells were isolated and cultured as described previously [10]. Primary ovarian cells were isolated and cultured base on the protocol described in Lesley D. Dunfield's publication [11]. All tissues were collected from Chongqing University Cancer Hospital. The project was approved by the ethics committee of Chongqing University Cancer Hospital (Chongqing, China) and in accordance with the Declaration of Helsinki. The written informed consents were obtained from each patient. The absence of mycoplasma was validated by e-Myco VALiD Mycoplasma PCR Detection Kit (25239, iNtRon Biotechnology, Brulington, MA, USA) and the cells were examined by short tandem repeat profiling.

2.2. Isolation of ovarian cancer stem like cells (OCSLCs)

Ovarian cancer stem-like cells (OCSLCs) were used as cell model for OCSCs study. The workflow of isolation and characterization of OCSLCs was provided in Fig. 1A. Briefly, the adherent parental cells were suspension cultured in ultra-low attachment culture dish/plate (3471/4520, Corning, Inc, Corning, NY, USA) containing OCSLCs culture medium (serum-free medium supplemented with 20 ng mL^{-1} recombinant human epidermal growth factor (rh-EGF, PHG0313, Thermo Fisher, Waltham, MA, USA), 10 ng mL^{-1} recombinant human basic fibroblast growth factor (rh-bFGF, PMG0033, Thermo Fisher, Waltham, MA, USA), and antibiotics). When the cells were cultured for 15 days or have reached 60% confluence, the cells were collected by centrifugation and washed for at least two times with Phosphate-buffered saline (PBS). CD133 + cells were separated by Magnetic Assisted Cell Sorting (MACS) technology (Miltenyi Biotech, Bergisch Gladbach, Germany) according to the manual. Briefly, the cells were first labelled with CD133-biotin antibody and incubated at 4 °C for 15 min. The labelled cells were then washed and further labelled with anti-biotin microbeads, followed by magnetic separation. ALHD+ cells were isolated by ALDEFLUOR™ Kit (Stem Cell Technologies, Canada) according to the manual. ALDEFLUOR™ Kit employs a fluorescent non-toxic ALDH substrate, BODIPY-aminoacetaldehyde (BAAA), as an indicator, which freely diffuses into viable cells. In the presence of ALDH, BAAA is converted into BODIPY-aminoacate (BAA) and retained inside the cells. Thus, viable ALDH-bright cells could be isolated by flow cytometry. The isolated CD44 +ALDH+ spheroid cells were named as OCSLCs and used as model for OCSCs study.

2.3. Compounds and plasmids

Luteolin was obtained from Sigma-Aldrich (L9283, St. Louis, MO, USA) and dissolved in dimethyl sulfoxide (DMSO, 276855, Sigma-Aldrich, St. Louis, MO, USA) at 150 mM as stock solution. Paclitaxel was purchased from Selleckchem (S1150, Houston, TX, USA) and dissolved in DMSO at 150 mM as stock solution. Carboplatin was obtained from Sigma-Aldrich (C2538, Sigma-Aldrich, St. Louis, MO, USA) and dissolved in ddH_2O at 10 mM as stock solution. KDM4C inhibitor SD70 was obtained from Sigma-Aldrich (5.31662, St. Louis, MO, USA) and was resolved in DMSO at 50 mg mL^{-1} as stock solution. Cycloheximide (CHX, C4859, 100 mg mL^{-1}) was purchased from Sigma-Aldrich (St. Louis, MO, USA). The concentration of DMSO used in cell-based assay was less than 0.1% and the amount of DMSO has not interfered with obtained results of experiments. Lentivirus plasmids pCDH-CMV-MCS-EF1-Puro and PLKO.1 puro were kindly provided by professor Hongbin Ji (Shanghai Institutes for Biological Sciences, Chinese Academy of Sciences, Shanghai, China). YAP-, PPP2CA- and KDM4C-overexprssing plasmids were constructed by inserting their coding sequences into pCDH-CMV-MCS-EF1-Puro plasmids. YAP5SA mutant was constructed by site-directed mutagenesis or deletion by PCR. shRNA-resistant KDM4C was obtained by inserting non-sense mutations in shRNA-targeting sites. Q5 sit-directed mutagenesis kit (E0054S, NEB, lpswich, MA, USA) was used to construct H190A/E912A mutant (demethylase dead) KDM4C. YAP- and KDM4C-knockdown plasmids were constructed by inserting specific shRNAs into PLKO.1 plasmids. The primers and shRNAs used in this study were listed in Tables S1 and S2. An 8xGTIIC-*luciferase plasmid (*#34615, *A*ddgene, Cambridge, MA, USA*)* was used to determine YAP transcriptional activity. A fluorescent TCF/LEF reporter lentivirus and the reporter plasmid for Hedgehog signaling pathway were kindly provided by professor Jiangfeng Qiu (Renji Hospital Shanghai Jiao Tong University School of Medicine, Shanghai, China). Common luciferase reporter gene assays were performed by pGL4.20 (E6751, Promega, Madison, WI, USA) plasmid. pRL Renilla luciferase control reporter vector (E2231, Promega, Madison, WI, USA) was used for normalization in reporter assays.

2.4. Real-Time Quantitative Reverse Transcription Polymerase Chain Reaction (qRT-PCR)

The qRT-PCR assays were performed according to the standard protocol. Briefly, Trizol reagent (10296010, Thermo Fisher, Waltham, MA, USA) was used for RNA isolation. Ethanal and residual DNA were removed by evaporation and Turbo DNAse (AM2239, Thermo Fisher, Waltham, MA, USA). The assay was finished by SuperScript™ III Platinum™ kit (11732088, Thermo Fisher, Waltham, MA, USA) according to the manual.

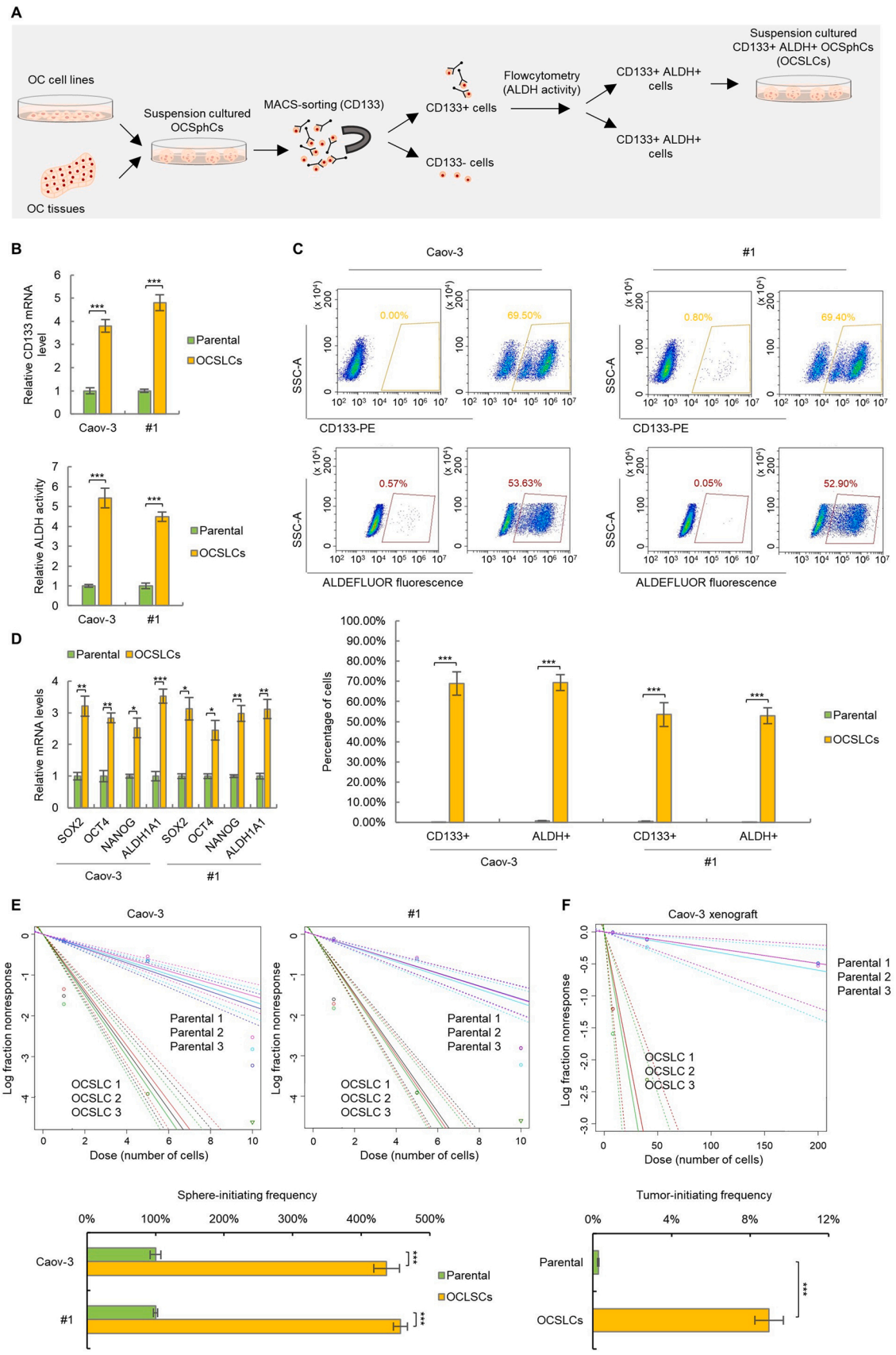

Fig. 1. Isolation and characterization of OCSLCs. (A) Workflow of isolation and characterization of OCSLCs. (B) qRT-PCR and Aldefluor assay analysis of CD133 expression and ALDH activity in indicated cells. (C) Flow cytometry analysis of the percentages of CD133 + and ALDH+ cells in indicated cells. (D) qRT-PCR analysis of the mRNA levels of stemness-related markers in indicated cells. (E,F) In vitro (E) and in vivo (F) limiting dilution analysis of sphere-initiating and tumor initiating capacities of indicated cells. Student's t test, *$P < 0.05$, *$P < 0.01$, *$P < 0.001$.

2.5. ALDH activity test

ALHD activity in the cells were examined by ALDEFLUOR™ Kit (Stem Cell Technologies, Canada) according to the manual. Briefly, the ALDEFLUOR™ reagent was activated first. The cells were collected, and the concentration was adjusted to 1 × 106 cells/mL with the ALDEFLUOR™ Assay Buffer. The substrate was then added, and the mixture was incubated for 60 min at 37 °C. After incubation, the cells were washed 2 times by centrifugation in ALDEFLUOR™ Assay Buffer. The signal in the cells was detected by plater reader.

2.6. Limiting dilution assay (in vitro)

The parental Caov-3 an #1 OC cancer cells were routinely cultured as mentioned above. OCSLCs were cultured in suspension culture condition in ultra-low attachment culture dish/plate containing OCSLCs culture medium (serum-free medium supplemented with growth factors as mentioned above). Before collection, the cells were treated according to the experimental design. The cells were collected by centrifugation and washed once by serum-free medium. Then, the cells were dissociated into singular cells. After dissociation, the cells were seeded into 96-well ultra-low attachment culture plate (Corning, NY, USA) at the density of one, five, ten cells per well (50 wells for each group). The next day, the presence of an indicated number of cells in each well was visually checked. After fifteen days, the number of wells containing spheroids were quantified by manual counting. Extreme limiting dilution assay analyses (ELDAs) were performed by ELDA online software designed by Hu and colleagues [12].

2.7. Drug sensitivity assay (in vitro)

The adherent cells or OCSLCs were collected, dissociated and counted, followed by culture in 96 well normal or ultra-low attached plates with the culture media containing different concentration of compounds for 48 h. CCK-8 assay kit (CK04, Dojindo Molecular Technologies, Tokyo, Japan) was employed to determine the cell number. Cell viability was calculated as absorbance((treated-blank)/(vehicle-blank))%. Inhibition rate was calculated as 1-viability. The half-maximal inhibitory concentration (IC_{50}) was determined by R package. Three independent experiments, triplicate for each, were performed.

2.8. Cell derived xenograft (CDX) model, limiting dilution assay (in vivo), and drug sensitivity assay (in vivo)

Female BALB/c nude mice (Pusheng Technology, Nanjing, China), 6–8 weeks of age, were used for development of CDX model and in vivo limiting dilution assay. The Caov-3 spheroid cells were used for determination of anti-tumor and sensitizing effect of luteolin in vivo. The Caov-3 derived OCSLCs were used in vivo limiting dilution assay. For development of CDX model for testing anti-tumor and sensitizing effects of luteolin, Caov-3 spheroid cells were collected and digested into single cells, followed by inoculation into the flank of the BALB/c nude mice at a density of 5×10^6 cells in 0.2 mL culture medium containing 25% Matrigel (CB-40234, Thermo Fisher, Waltham, MA, USA). To evaluate the anti-tumor effect of luteolin, 100 mg kg^{-1} luteolin (single dose per week) was administered. For testing sensitizing effect of luteolin, 0.3 mg kg^{-1} luteolin (single dose per week), 40 mg kg^{-1} Carboplatin (single dose per week), and 15 mg kg^{-1} paclitaxel (single dose per week) were administered. The drugs were administrated intravenously, and the equal volume of corresponding vehicle was used as control. The tumor volume (length × $width^2/2$) was observed every 7 days. One mouse in each group was sacrificed at day 21 for imaging. The rest were sacrificed when the length of the tumor ≥ 20 mm or the volume of tumor = 2000 mm^3 for survival analysis. Inhibition rate was calculated as 100% × (tumor volume $_{vehicle}$ – tumor volume $_{treated}$) / tumor volume $_{vehicle}$. The survival analysis was performed using R package. For in vivo limiting dilution assay, the cells were first treated according to the experimental design, followed by inoculation into the flank of the BALB/c nude mice at a density of 8, 40, and 200 cells per mouse (10 mice for each group). The tumors were monitored every week, and the number of mice bearing tumor was quantified at the endpoint. Extreme limiting dilution assay analyses (ELDAs) were performed by ELDA online software designed by Hu and colleagues [12].

2.9. Sphere-formation assay

The parental Caov-3 an #1 OC cancer cells were routinely cultured as mentioned above. The cells were collected by centrifugation and washed once by serum-free medium. Then, the cells were dissociated into singular cells. After dissociation, the cells were seeded into 6-well ultra-low attachment culture plate (3471, Corning, NY, USA) at the density of 3000 cells / well and cultured in OCSLCs culture medium containing indicated drugs. After 48 h treatment, the medium was changed into fresh OCSLCs culture medium and the cells were continually cultured for another 13 days in suspension culture condition for sphere formation. For YAP-, PPP2CA-, KDM4C-overexpressing OCSLCs, the cells were cultured 11 days after treatment. The spheroids were quantitated using inverted phase-contrast microscopy and photographed.

2.10. Cell viability

Cell viability was assessed by using Trypan blue exclusion assay [13].

2.11. Luciferase reporter assay

The reconstructed plasmids were transfected into cells together with pRL-TK plasmids. Dual-luciferase reporter assay system (e1901 Promega Corporation, Madison, WI, USA) was used to determine the luciferase activity.

2.12. Western blot and protein degradation

The western blot assays were performed according to the standard protocol. The detailed information of antibodies used in this study was given in Table S3. To determine the degradation of the proteins, the cells were first treated according to the experimental design (genetic manipulation or compound treatment), followed by inhibition of translation with CHX (10 μM, 4 h). The cells were further cultured for 12 or 24 h, followed by determination of protein levels by western blot. The degradation rate was calculated as blot density(target/internal control)$_{((start\text{-}end)/start)}$%. Three independent experiments, triplicate for each, were performed. Uncropped gels were provided in supplementary materials.

2.13. Nuclear run-on assay

The nuclear run-on assay was performed according to Stephen T Smale's publication [14] with some modification and Click-iT® Nascent RNA Capture Kit (C10365, Thermo Fisher, Waltham, MA, USA) was employed in this study. Briefly, the OCSLCs were collected and dissociated into singular cells. The dissociated cells were suspension cultured at the density of 0.5 million per milliliter (mL). After 8 h culture, the cells were treated with the maximal non-toxic dose of luteolin or vehicle for 48 h. Then, 0.5 mM 5-ethynyl Uridine (EU) (0.5 mM) was added into the culture medium and the cells were cultured for another 1 h. The cells were harvested and washed, followed by RNA isolation. The total RNA was routinely isolated by TRIzol™ reagent (15596026, Thermo Fisher, Waltham, MA, USA). The high-quality mRNA was prepared using the Poly(A)Purist mRNA purification kit (AM1922, Thermo Fisher, Waltham, MA, USA). Biotinylation of RNA was performed by mixing water, Click-iT ® EU buffer, Copper (II) Sulfatte (CuSO4), Biotin azide, EU-RNA, Click-iT® reaction buffer additive 1, Click-iT® reaction buffer

additive 2, according to the manual. The mixture was incubated for 30 min by gently vortex. The biotinylated RNA was routinely precipitated and collected by ethanol. Next, the biotinylated RNA was purified by Dynabeads® MyOne™ Streptavidin T1 magnetic beads according to the manual. Finally, the biotinylated EU-labeled RNA was subjected to cDNA synthesis for qRT-PCR.

2.14. Chromatin immunoprecipitation PCR (ChIP-PCR) assay

MAGnify™ Chromatin Immunoprecipitation System was employed for ChIP-PCR assay in this study and the work from John Arne Dahl and colleagues [15] was also referred. Briefly, the cells were cultured in suspension culture condition at the density of 100,000 cells per well. After treatment, the cells were collected by centrifugation. The beads were prepared by coupling the antibodies to the Dynabeads®. The cells were resuspended in 500 microliters (μL) Phosphate-buffered saline (PBS). Then, 13.5 μL of 37% formaldehyde was added and the cells were incubated for 10 min at room temperature. The reaction was stopped by addition of 57 μL of 1.25 M glycine. The cells were collected and washed, followed by lysis with lysis buffer (the final concentration of cells in lysis buffer was 1 million cells per 50 μL). Then, the chromatin was sheared into 200–500-bp fragments by sonication. After dilution of the chromatin according to the manual, antibody-Dynabeads ® were used to bind the chromatin linked with the target protein (this step was performed according to the mannual). The bound chromatin was subsequentially washed with IP buffer 1 and IP buffer 2, followed by elution by reversing the crosslinking between chromatin and target protein. Finally, the DNA was purified and subjected into further analysis.

2.15. Binding prediction using online software

The binding between luteolin and KDM4C was predicted by Click Docking online software (https://mcule.com/dashboard/) according to the manual.

2.16. Binding Assay using luteolin-conjugated beads

Photoaffinity linker-coated agarose beads (1st generation) were prepared as the description in publication by Naoki Kanoh and colleagues [16]. Briefly, N-Hydroxysuccinimidyl (NHS)-activated agarose was purchased from Thermo Scientific (26196, Thermo Fisher, Waltham, MA, USA). The 1st generation photoaffinity linkers were synthesized with *N-tert*-butoxycarbonyl-2,2'-ethylenedioxy-bis(ethylamine) and 4-[3-(trifluoromethyl)− 3*H*-diazirin-3-yl] benzoic acid according to the procedure reported by Naoki Kanoh and colleagues [17]. *N-tert*--butoxycarbonyl-2,2'-ethylenedioxy-bis(ethylamine) was synthesized according to the method reported by Beer P D et al. [18]. The photoaffinity linkers were coupled with NHS- activated agarose according to the manual and publication by Naoki Kanoh and colleagues [16]. The luteolin beads were prepared base on the publication from Kawatani M et al. [19]. Briefly, the photoaffinity linker-coated agarose beads were transferred to a spin column for washing with distilled water. After removing the residual water by a rotary evaporator, the beads were suspended in 2-propanol in a glass sample vial, followed by desiccation in vacuo. Then, a solution of luteolin (1 mg/150 μL) was added to the beads, followed by mixing, concentration and desiccation in vacuo. The beads were then irradiated with 365 *nm* UV light at 4 J per cm^2, followed by wash successively with 50% methanol, methanol, DMSO, and methanol. The resulting beads were maintained in PBS. The binding assay was performed according to the publication from Li J et al. [20] with some modification. Briefly, the cells were lysed and homogenized by a syringe in binding buffer (10 mM Tris-HCl (pH 7.6), 4 mM $MgCl_2$, 40 mM KCl, 1 mM EDTA, and protease inhibitor cocktail). The luteolin beads or control beads were then added into cell lysate and incubation for 12 h at 4 °C. The beads were then boiled in sample loading buffer (#7722, Cell Signaling Technology, Boston, MA, USA), followed by short centrifugation. The supernatant was then analysis by western blot assay.

2.17. Statistics

Data were represented as 'mean ± SD'. Student's t-test and One-way ANOVA were applied for evaluation of differences between two or three groups, respectively. All analyses were unpaired and two-tailed (*$P < 0.05$, **$P < 0.01$, ***$P < 0.001$).

3. Results

3.1. Isolation and characterization of OCSLCs

Previous studies have shown that OCSCs exhibit elevated CD133 expression, ALDH activity, in vitro sphere-initiating capacity and in vivo tumor-initiating capacity [21–23]. We thus isolated $CD133^+$ $ALDH^+$ spheroid cells (named as OCSLCs) from adherent cultured parental Caov-3 cell line and #1 primary OC cell as OCSCs model (Fig. 1A). The result from qRT-PCR analysis showed that the mRNA level of CD133 was significantly increased in OCSLCs versus parental cells (Fig. 1B, n = 3, $P < 0.001$ in Caov-3 and #1 cells). The result from ALDH activity assay showed that the ALDH activity was significantly increased in OCSLCs versus parental cells (Fig. 1B, n = 3, $P < 0.001$ in Caov-3 and #1). The percentages of CD133 + cells and ALDH+ cells were also increased in OCSLCs versus parental cells (Fig. 1C, n = 3, $P < 0.001$ for CD133 + cells in Caov-3 and #1; n = 3, $P < 0.001$ for ALDH+ cells in Caov-3 and #1) as identified by flow cytometry. The expression of other recognized CSCs markers, including SOX2, OCT4, NANOG, and ALDH1A1, were also increased in OCSLCs versus parent cells (Fig. 1D, n = 3, $P < 0.05$ for NANOG, $P < 0.01$ for SOX2, OCT4, $P < 0.001$ for ALDH1A1 in Caov-3, $P < 0.05$ for SOX2 and OCT4, $P < 0.01$ for NANOG and ALDH1A1 in #1) as identified by qRT-PCR. In addition, the in vitro sphere-initiating capacity was significantly increased in OCSLCs versus parental cells (Fig. 1E and Supplementary Fig. 1A, 3 replicates, $P < 0.001$ in both) as identified by in vitro limiting dilution assay; no significant difference in cell viability was observed between the spheres derived from OCSLCs and parental cells (Supplementary Fig. 1B, n = 3, $P > 0.05$ in both). Furthermore, the tumor-initiating capacity was also significantly increased in Caov-3 OCSLCs versus parental cells (Fig. 1F and Supplementary Fig. 1C, 3 replicates, $P < 0.001$) as identified by in vivo limiting dilution assay. Similarly, no significant difference in cell viability was observed between the xenografts derived from OCSLCs and parental cells (Supplementary Fig. 1D, n = 3, $P > 0.05$). Importantly, the percentage of CD133 + and ALDH+ cells was significantly higher in xenografts derived from OCSLCs versus parental cells (Supplementary Fig. 1E, n = 3, $P < 0.001$). Taken together, these results support that the isolated OCSLCs could be served as OCSLCs model.

3.2. Luteolin inhibits the stemness of OCSLCs

We next investigated the inhibitory effect of luteolin on adherent OC cells, OCSLCs, and normal human cells. As shown in Fig. 2A, a diagram of determination of the inhibitory effect of luteolin on OCSLCs, luteolin-induced reduction in the cell number of spheres depends on both stemness inhibition and viability inhibition [24,25]. The results from CCK-8 assay showed that the IC50 values of luteolin in adherent cultured parental Caov-3 and #1 cells are 40.89 and 38.01 μM (Fig. 2B, n = 3). This result is consistent with the observations in other types of cancer cells: human esophageal squamous carcinoma cell line Eca109 (70.70 μM) [26], human cervical cancer cell line Hela (15.41 μM) [27], human bone osteosarcoma epithelial cell line U2OS (36.35 μM) [4], human prostate cancer cell line PC-3 (25.25 μM) [28], human colorectal cancer cell line HCT-116 (25.00 μM) [29]. We next found that OCSLCs are inherently resistant to luteolin; the IC50 values of luteolin are 141.00 μM in Caov-3 OCSLCs and 136.20 μM in #1 OCSLCs (Fig. 2B,

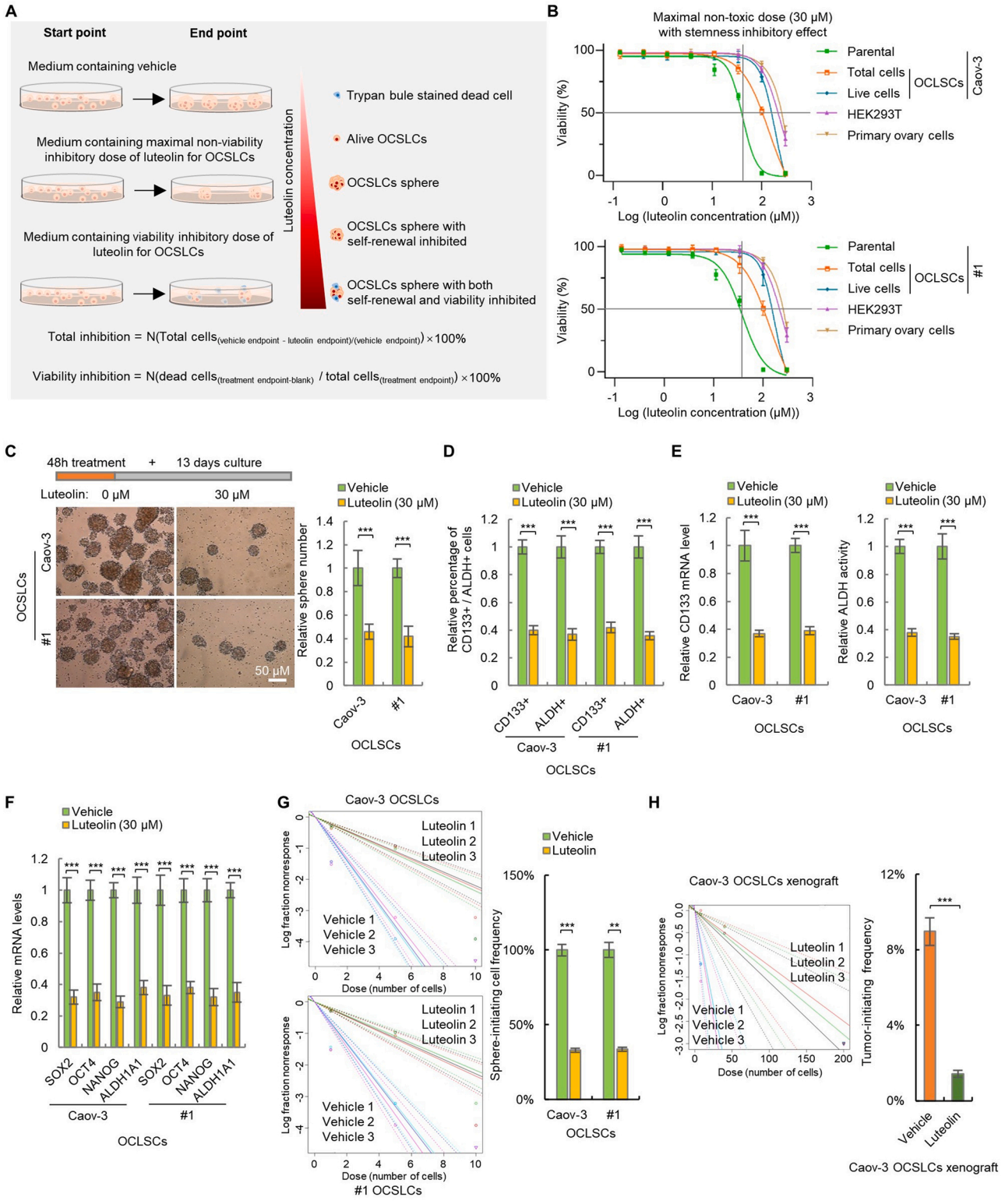

Fig. 2. Luteolin inhibits the stemness of OCSLCs. (A) Diagram illustrating stemness and viability inhibition in OCSLCs. (B) IC_{50} values of luteolin in adherent parental OC cells, OCSLCs, normal cells. (C) Sphere-formation assay analysis of sphere-forming capacities of indicated cells. (D) Flow cytometry analysis of the percentages of CD133 + and ALDH+ cells in indicated cells. (E) qRT-PCR and Aldefluor assay analysis of CD133 expression and ALDH activity in indicated cells. (F) qRT-PCR analysis of the mRNA levels of stemness-related markers in indicated cells. (G,H) In vitro (G) and in vivo (H) limiting dilution analysis of sphere-initiating and tumor initiating capacities of indicated cells. Student's t test, $^{*}P < 0.05$, $^{*}P < 0.01$, $^{*}P < 0.001$.

n = 3). This result is consistent with the general theory that CSCs are naturally resistant to cytotoxic agents [30–33] and indicates the inhibitory effect of luteolin on OCSLCs. Moreover, normal cells were found to be more tolerant than OCSLCs to luteolin; the IC50 values of luteolin in HEK293T and primary normal human ovarian cells were 231.90 and 258.50 μM, respectively (Fig. 2B, n = 3). This result is consistent with the observations from Kim YS and colleagues [4] and indicates the tolerance of luteolin. Furthermore, we found that although luteolin led to a considerable reduction in total number of cells in both Caov-3 and #1 OCSLCs at the concentration of 30 μM, no significant difference in cell viability (dead/live rate) was observed (Fig. 2B, n = 3), which indicates that only the stemness, but not the viability, was inhibited at this concentration. Thus, we chose 30 μM (the maximal non-toxic dose) for further mechanistic study. Taken together, these results suggest that luteolin inhibits both adherent OC cells and OCSLCs, OCSLCs are more resistant to luteolin than adherent OC cells, lower concentration of luteolin is needed for stemness inhibition compared with viability inhibition in OCSLCs, and normal cells are more tolerant than tumorigenic cells.

Next, to confirm the stemness inhibitory effect of luteolin in OCSLCs, we examined the sphere-forming capacity, marker expression, percentage of CD133 +ALDH+ cells, as well as sphere-initiating and tumor-initiating capacity of OCSLCs treated with the maximal non-toxic dose (30 μM) of luteolin. As expected, without difference in cell viability (Supplementary Fig. 1A, n = 3, $P > 0.05$ in Caov-3 and #1 OCSLCs), OCSLCs treated with the maximal non-toxic dose of luteolin exhibited significantly lower sphere-forming capacity (Fig. 2C, n = 3, $P < 0.001$ in both), percentage of CD133 + and ALDH+ cells (Fig. 2D, n = 3, $P < 0.001$ for CD133 + and ALDH+ in both). In addition, the expression of CD133, ALDH activity (Fig. 2E, n = 3, $P < 0.001$ for CD133 and ALDH activity in both) as well as the expression of all selected stemness markers (Fig. 2F, n = 3, $P < 0.001$ for all markers in both) were significantly decreased in OCSLCs treated with the maximal non-toxic dose of luteolin versus OCSLCs treated with vehicle. Moreover, in vitro sphere-initiating capacity (Fig. 2G and Supplementary Fig. 2B, 3 replicates, $P < 0.001$ in both) and in vivo tumor-initiating capacity (Fig. 2H and Supplementary Fig. 2C, 3 replicates, $P < 0.001$ in #1) were significantly decreased in luteolin-treated OCSLCs versus vehicle-treated control OCSLCs. Furthermore, the xenograft derived from luteolin-treated OCSLCs exhibited lower percentage of CD133 + and ALDH+ cells versus xenograft derived from vehicle-treated OCSLCs (Supplementary Fig. 2D, n = 3, $P < 0.001$ for CD133 + and ALDH+). Similarly, no differences in cell viability were observed between spheres and xenografts derived OCSLCs treated with luteolin and vehicle (Supplementary Fig. 2E and F, $P > 0.05$ in all). These results thus support that the maximal the non-toxic dose of luteolin inhibits the stemness of OCSLCs.

3.3. Hippo/YAP signaling is the downstream target of luteolin

Wnt, Hippo/YAP, and Hedghog signaling pathways primarily associate with stemness regulation in both normal and cancer cells [34]. We thus first investigated whether luteolin regulates these pathways in OCSLCs. The result from qPCR-array showed that the maximal non-toxic dose of luteolin inhibited the expression of most downstream target genes of Hippo/YAP pathway in OCSLCs (Fig. 3A, n = 3, $P < 0.05$ for all genes). The result from luciferase reporter assay showed that the maximal non-toxic dose of luteolin significantly inhibited the transcriptional activity of YAP (Fig. 3B, n = 3, $P < 0.001$ in both). While, no significant differences in the expression of the target genes of Wnt signaling (Fig. 3C, n = 3, $P > 0.05$ for all), TCF transcriptional activity (Fig. 3D, n = 3, $P > 0.05$ for all), the expression of the target genes of Hedghog signaling (Fig. 3E, n = 3, $P > 0.05$ for all), and HH activity (Fig. 3F, n = 3, $P > 0.05$ for all) were observed in OCSLCs treated with the maximal non-toxic dose of luteolin. These results motivated us to speculate that inhibition of Hippo/YAP signaling is the mechanism underlying luteolin inhibiting OCSLCs stemness.

Hippo signaling is an evolutionarily conserved pathway that regulates cell proliferation, apoptosis, and stem cell self-renewal by phosphorylating YAP and TAZ, two transcription co-activators [35]. Phosphorylated YAP and TAZ undergo degradation, while unphosphorylated YAP and TAZ translocate into nucleus and activate gene transcription [35]. YAP and TAZ were also regulated by other enzymes, such as PPP2CA (Protein Phosphatase 2 Catalytic Subunit Alpha) [35]. To confirm the inhibitory effect of luteolin on YAP in OCSLCs, we next found that the abundance of nuclear YAP was significantly decreased in OCSLCs treated with the maximal non-toxic dose of luteolin by both western blot (Fig. 3G, n = 3, $P < 0.001$ in both cells) and immunostaining assay (Fig. 3H, n = 3, $P < 0.001$ in both). In addition, the nascent mRNA level of YAP target genes, CTGF and AREG [35], were significantly decreased in OCSLCs treated with the maximal non-toxic dose of luteolin as identified by nuclear run-on assay (Fig. 3I, n = 3, $P < 0.001$ for CTGF and AREG in both cells). Together with the observation that luteolin reduced the transcriptional activity of YAP (Fig. 3B), these results support that luteolin inhibits Hippo/YAP signaling in OCSLCs.

To investigate the mechanism underlying luteolin inhibiting Hippo/YAP signaling, we next found that treatment with the maximal non-toxic dose of luteolin had no effect on the mRNA level of YAP (Fig. 3J, n = 3, $P > 0.05$ for all) in OCSCs. While, the abundance cytoplasmic YAP and TAZ was significantly decreased (Fig. 3K, n = 3, $P < 0.001$ for both YAP and TAZ). Meanwhile, the levels of phosphorylated YAP and TAZ were significantly increased (Fig. 3L, n = 3, $P < 0.001$ for both YAP and TAZ), which indicates that the reduced protein level of YAP and TAZ may be the result of luteolin-induced accelerated degradation. This hypothesis was further confirmed by detecting the protein level in YAP and TAZ in OCSLCs treated with CHX for inhibition of translation. We found that after CHX treatment OCSLCs, the protein levels of YAP and TAZ in luteolin-treated OCSLCs were significantly decreased versus non-treated OCSLCs (Supplementary Fig. 3A). Taken together, these results demonstrated that luteolin inhibits Hippo/YAP signaling in OCSLCs; and promoting YAP and TAZ degradation is the prime mechanism.

3.4. Luteolin inhibits OCSLCs stemness by suppressing Hippo/YAP signaling

To confirm the critical role of suppression of Hippo/YAP signaling in luteolin inhibiting the stemness of OCSLCs, we induced YAP-independent OCSLCs (Fig. 4A). The YAP in Caov-3 cells was first depleted by shRNAs. The YAP-knockdown cells with high stemness properties were subsequentially selected by single cell clone selection. The efficiency of YAP knockdown was demonstrated by western blot (Supplementary Fig. 4A). As expected, the stemness inhibitory effect of luteolin in OCSLCs was, at least partially, abolished as reflected by the restored sphere-forming capacity (Fig. 4B, n = 3, $P < 0.001$), percentage of CD133 + and ALDH+ cells (Fig. 4C, n = 3, $P < 0.001$ for both CD133 + and ALDH+), CD133 expression and ALDH activity (Fig. 4D, n = 3, $P < 0.001$ for all), the expression of stemness markers (Fig. 4E, n = 3, $P < 0.001$ for all), in vitro sphere-initiating capacity (Fig. 4F and Supplementary Fig. 4B, WT-luteolin 1:4.55 vs. YAP-independent-luteolin 1:2.66 in Caov-3, WT-luteolin 1:4.48 vs. YAP-independent-luteolin 1:2.51 in #1, $P < 0.001$ in both), as well as in vivo tumor-initiating capacity (Fig. 4G and Supplementary Fig. 4C, WT-luteolin 1:71.4 vs. YAP-independent-luteolin 1:15.1, $P < 0.001$). Consistently, the percentages of CD133 + and ALDH+ cells were significantly restored in xenograft derived from luteolin-treated YAP-independent Caov-3 OCSLCs (Supplementary Fig. 4D, n = 3, $P < 0.001$). Furthermore, no differences in cell viability were observed in sphere-formation, in vitro and in vivo limiting dilution assays (Supplementary Fig. 4E-G, $P > 0.05$ in all).

We next examined the stemness inhibitory effect of luteolin in OCSLCs with overexpression of wild-type YAP and YAP5SA. Similar

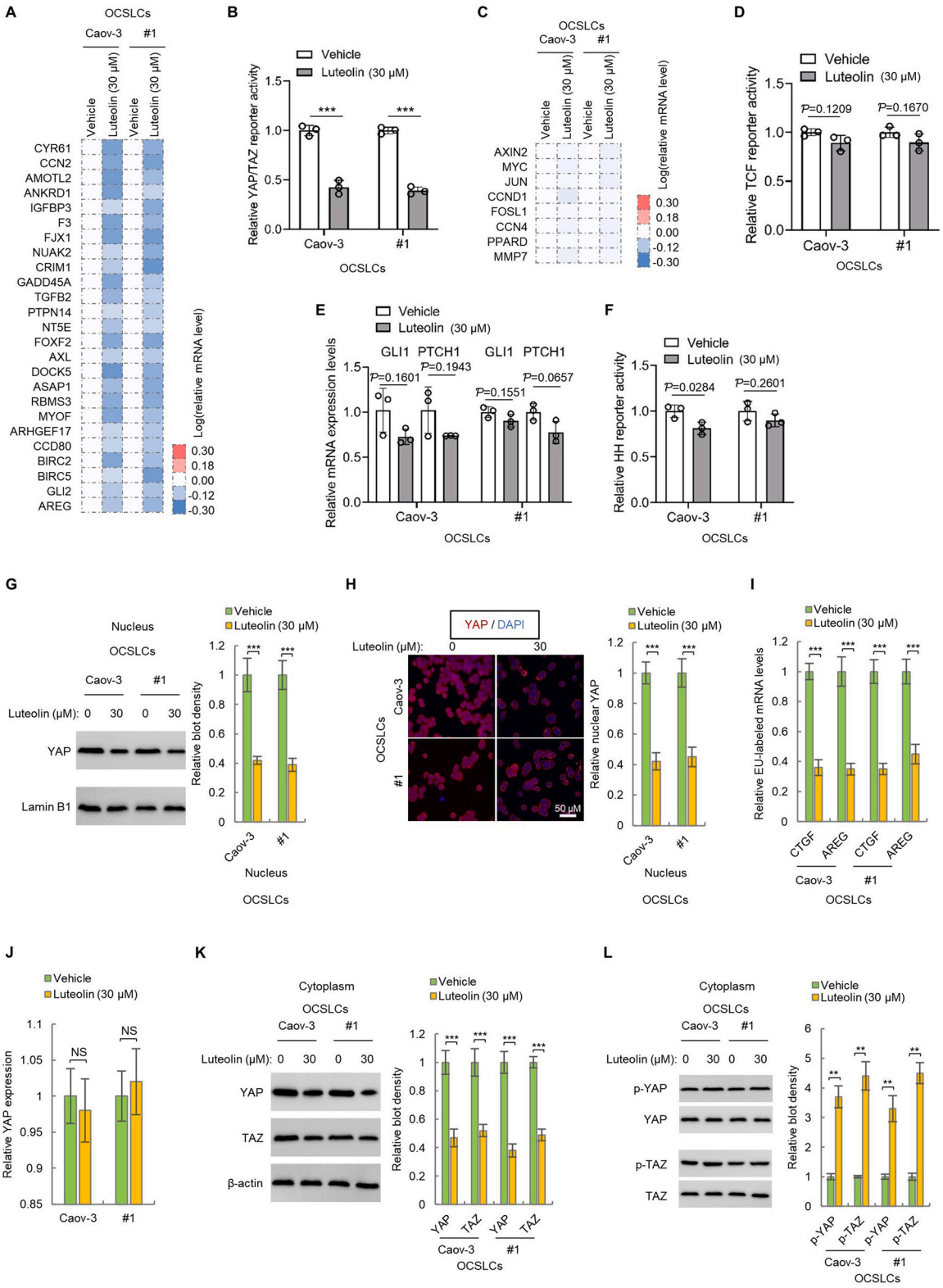

Fig. 3. Hippo/YAP signaling is the downstream target of luteolin. (A,C,E) qRT-PCR analysis the mRNA levels of the target genes of Hippo/YAP (A), Wnt (C), and Hedgehog (E) signaling pathways. (B,D,F) Luciferase reporter assay analysis of the transcriptional activity of YAP (B), TCF (D), and Hedgehog signaling (F). (G) Western blot analysis of the protein levels of YAP in indicated cells. (H) Immunostaining analysis of YAP sublocation in indicated cells. (I) Nuclear run-on assay analysis of the nascent mRNA levels of CTGF and AREG in indicated cells. (J) qRT-PCR analysis of YAP mRNA levels in indicated cells. (K,L) Western blot analysis of the protein levels of YAP, TAZ, phosphorylated YAP, and phosphorylated TAZ in indicated cells. Student's t test, *$P < 0.05$, *$P < 0.01$, *$P < 0.001$.

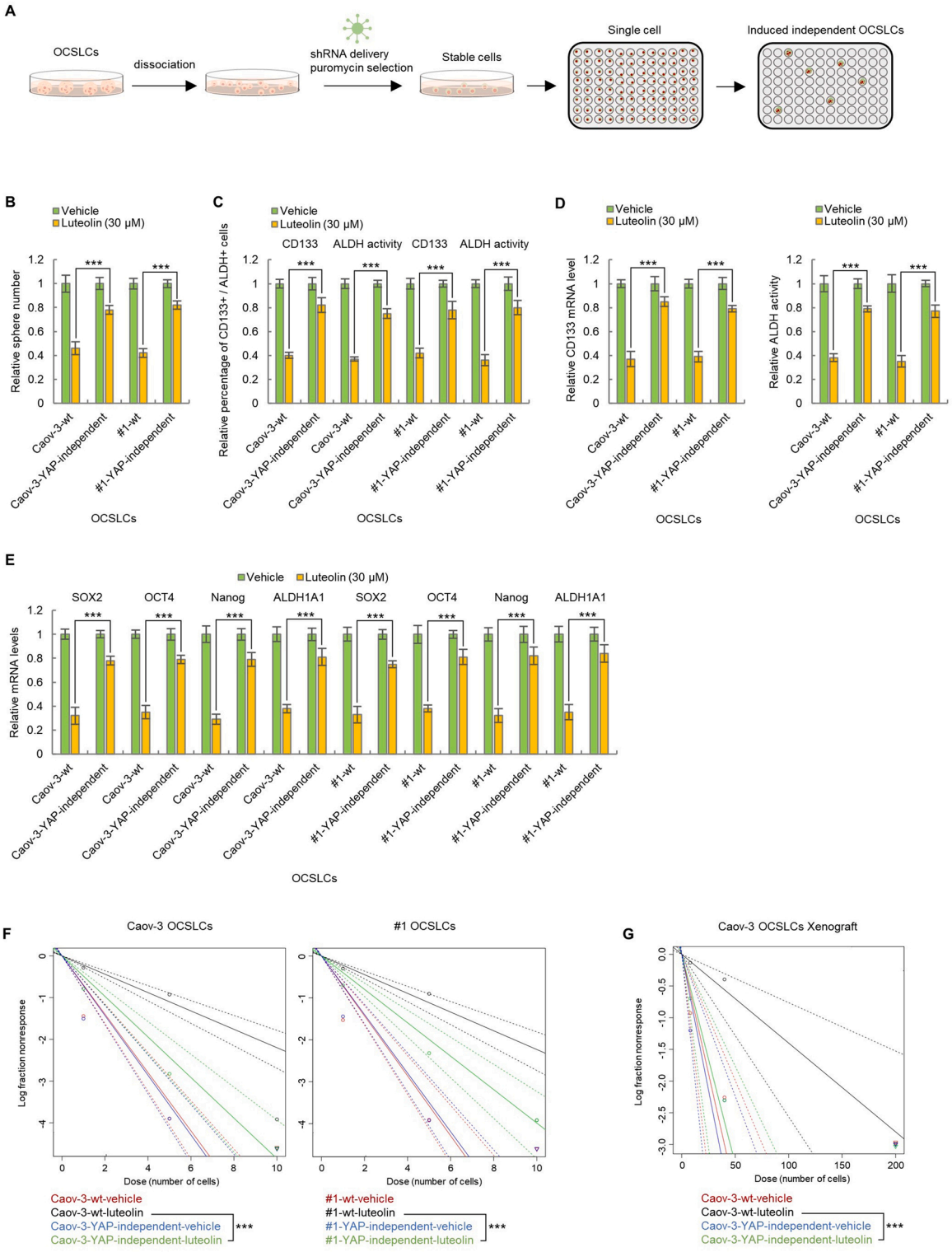

Fig. 4. YAP-independent OCSLCs are resistant to luteolin. (A) Workflow of development of YAP-independent OCSLCs. (B) Sphere-formation assay analysis of sphere-forming capacities of indicated cells. (C) Flow cytometry analysis of the percentages of CD133 + and ALDH+ cells in indicated cells. (D) qRT-PCR and Aldefluor assay analysis of CD133 expression and ALDH activity in indicated cells. (E) qRT-PCR analysis of the mRNA levels of stemness-related markers in indicated cells. **(F,G)** In vitro **(F)** and in vivo **(G)** limiting dilution analysis of sphere-initiating and tumor initiating capacities of indicated cells. One-way ANOVA analysis, $*P < 0.05$, $*P < 0.01$, $*P < 0.001$.

with the results in YAP-knockdown OCSLCs, OCSLCs with wild-type YAP overexpression (Supplementary Fig. 5A) are resistant to luteolin as reflected by the restored sphere-forming capacity (Fig. 5A, n = 3, $P < 0.001$ in both cells), percentages of CD133 + and ALDH+ cells (Fig. 5B, n = 3, $P < 0.001$ for both CD133 + and ALDH+ in both cells), expression of CD133 (Fig. 5C, n = 3, $P < 0.001$ in both cells), ALDH activity (Fig. 5D, n = 3, $P < 0.001$ in both cells), stemness markers (Fig. 5E, n = 3, $P < 0.001$ for all markers in both cells), in vitro sphere-

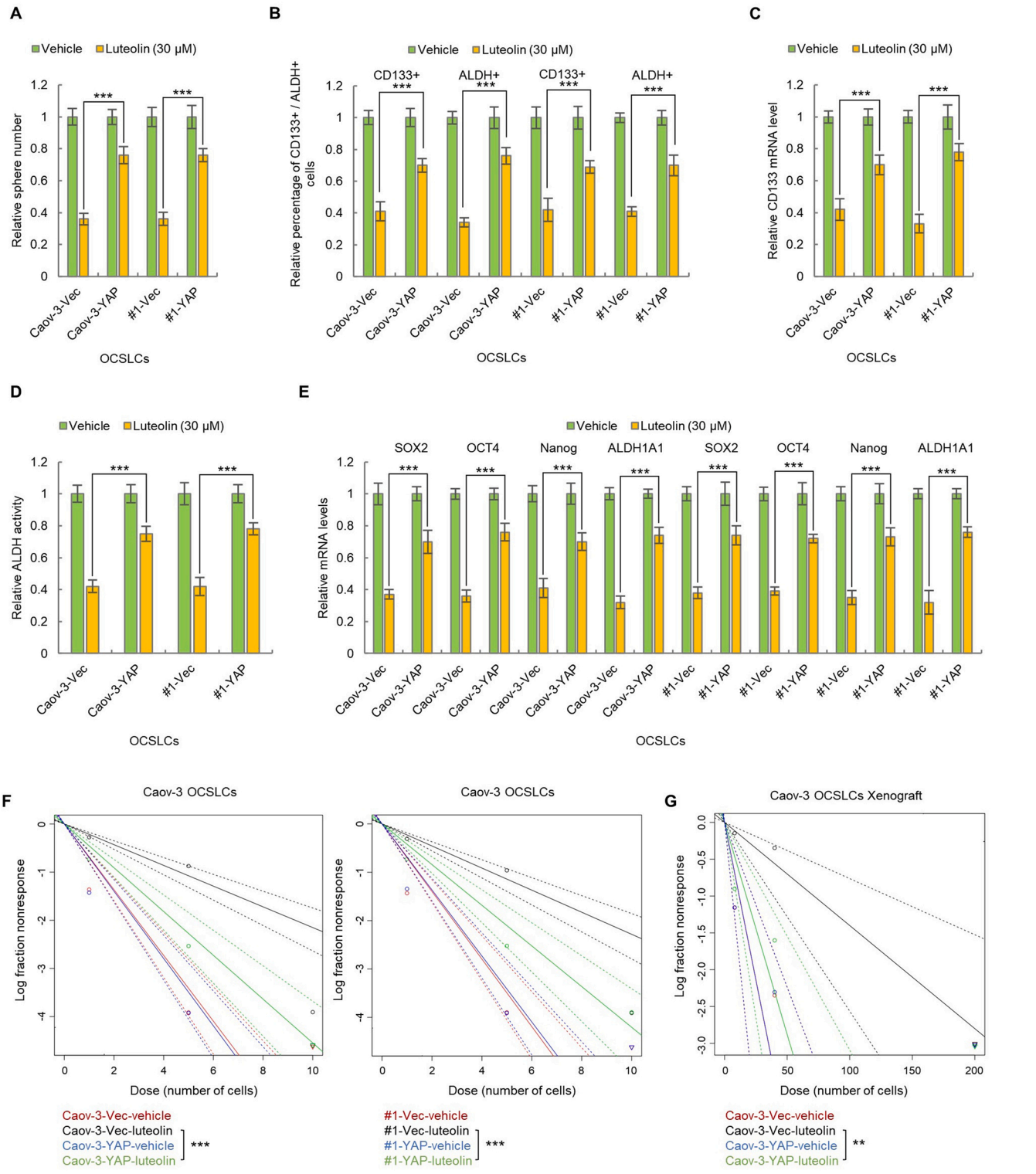

Fig. 5. YAP overexpression abolished the inhibitory effect of luteolin on the stemness of OCSLCs. (A) Sphere-formation assay analysis of sphere-forming capacities of indicated cells. (B) Flow cytometry analysis of the percentages of CD133 + and ALDH+ cells in indicated cells. (C,D) qRT-PCR (C) and Aldefluor assay analysis (D) of CD133 expression and ALDH activity in indicated cells. (E) qRT-PCR analysis of the mRNA levels of stemness-related markers in indicated cells. (F,G) In vitro (F) and in vivo (G) limiting dilution analysis of sphere-initiating and tumor initiating capacities of indicated cells. One-way ANOVA analysis, *$P < 0.05$, *$P < 0.01$, *$P < 0.001$.

initiating capacity (Fig. 5F and Supplementary Fig. 5B, Vec-luteolin 1:4.65 vs. YAP -luteolin 1:2.20 in Caov-3; Vec-luteolin 1:4.38 vs. YAP -luteolin 1:2.38 in Caov-3, $P < 0.001$ in both cells), and in vivo tumor-initiating capacity (Fig. 5G and Supplementary Fig. 5C, Vec-luteolin 1:71.4 vs. YAP-luteolin 1:17.4, $P < 0.001$ in both cells). The percentages of CD133 + and ALDH+ cells were significantly restored in xenograft derived from luteolin-treated YAP-overexpressing Caov-3 OCSLCs (Supplementary Fig. 5D, n = 3, $P < 0.001$). No differences in cell viability were observed in sphere-formation, in vitro and in vivo limiting dilution assays (Supplementary Fig. 5E-G, $P > 0.05$ in all). The

similar results were obtained in OCSLCs with overexpression of YAP5SA (Supplementary Fig. 6). Taken together, these results demonstrated that luteolin inhibits the stemness of OCSLCs, at least partially, though inhibition of Hippo/YAP signaling.

3.5. Luteolin inhibits Hippo/YAP signaling by transcriptional inhibition of PPP2CA

We next investigated the mechanism underlying luteolin suppressing Hippo/YAP signaling pathway. Based on above observation, it can be deduced that luteolin promotes the degradation of YAP and TAZ. We thus first speculated that luteolin regulates the expression of the upstream regulators of YAP. By qRT-PCR array, we found that luteolin inhibits the mRNA level PPP2CA in Caov-3 OCSLCs (Fig. 6A, n = 3, $P < 0.001$ for PPP2CA; $P > 0.05$ for rest genes in Caov-3). This result was further confirmed in OCSLCs derived from primary OC cells (Fig. 6B, n = 3, $P < 0.001$ in both cells). To confirm that luteolin inhibits the expression of PPP2CA at the transcriptional level, we examined the nascent mRNA level and the stability of PPP2CA in luteolin-treated OCSLCs. As expected, the nascent mRNA level of PPP2CA was significantly decreased in luteolin-treated OCSLCs versus control OCSLCs (Fig. 6C, n = 3, $P < 0.001$ in both cells). While no difference in stability of PPP2CA was observed in luteolin-treated OCSLCs (Fig. 6D). These results support that the transcription of PPP2CA is inhibited by luteolin in OCSLCs.

Next, to confirm that luteolin inhibits Hippo/YAP signaling pathway and stemness by suppressing PPP2CA, the OCSLCs derived from PPP2CA-overexpressing Caov-3 stable cell line was developed (Supplementary Fig. 7A). We found that overexpression of PPP2CA abolished the effect of luteolin on the protein level of nuclear YAP (Fig. 6E, n = 3, $P < 0.001$), the protein level of phosphorylated YAP (Fig. 6F, n = 3, $P < 0.001$), and the mRNA levels of YAP target genes (CTGF and AREG) (Supplementary Fig. 7B, n = 3, $P < 0.001$ for both) in Caov-3 OCSLCs. These results demonstrated that PPP2CA suppression is necessary for luteolin inhibiting Hippo/YAP signaling in OCSLCs. Furthermore, PPP2CA overexpression abolished the effect of luteolin on the stemness of OCSLCs (Fig. 6G-6 J and Supplementary Fig. 7C-E). These results support that PPP2CA suppression is necessary for luteolin inhibiting Hippo/YAP signaling and the stemness of OCSLCs.

3.6. Luteolin directly binds to KDM4C and inhibits PPP2CA transcription through suppressing KDM4C-mediated H3K9 demethylation in PPP2CA promoter region

Since above observations indicated that luteolin inhibits the transcription of PPP2CA, we next investigated the underlying mechanisms. According to the ENCODE transcription Factor Targets Dataset [36], histone marks H3K9me3, H3K36me3, H3K27ac are potential marks associated with PPP2CA transcription. Additionally, transcription factors CTGF, EP300, and POLR2A appears engaged to the promoter region of PPP2CA (Fig. 7A). We next employed ChIP-qPCR to investigate the histone marks or transcription factors associated with the stemness inhibitory effect of luteolin in OCSLCs. The results from ChIP-qPCR showed that only the abundance of H3K9me3 in PPP2CA promoter region was significantly increased in OCSLCs treated with the maximal non-toxic dose of luteolin versus OCSLCs treated with vehicle (Fig. 7B). Furthermore, we performed a binding assay by employment of luteolin-conjugated beads and found that KDM4C, a histone H3K9 demethylase, was eluted from luteolin-conjugated beads but not control beads (Fig. 7C), which indicated that luteolin directly binds to KDM4C. Similar result was obtained from the prediction by online software (Click Docking) which indicates that luteolin binds to the pocket of KDM4C (Fig. 7D). These results motivated us to investigate the role of KDM4C in intrinsic and luteolin-induced regulation of PPP2CA transcription. We next found that the mRNA level of PPP2CA was significantly increased in KDM4C-overexpressing cells (Supplementary Fig. 8A) versus control cells (Fig. 7E, n = 3, $P < 0.001$ for both). Oppositely, the mRNA level of PPP2CA was significantly decreased in KDM4C-knockdown cells versus control cells (Fig. 7E, n = 3, $P < 0.001$ for both). Moreover, the decreased mRNA level of PPP2CA in KDM4C-knockdown cells was restored by wild-type shRNA resistant KDM4C, but not H190A/E912A mutant (demethylase dead) shRNA resistant KDM4C (Fig. 7F, n = 3, $P < 0.001$ in both). Furthermore, wild-type shRNA resistant KDM4C, but not mutant shRNA resistant KDM4C, restored luteolin-induced decreased mRNA level of PPP2CA (Fig. 7G, n = 3, $P < 0.01$ in both), sphere-forming capacity (Fig. 7H, n = 3, $P < 0.01$), percentages of CD133 + and ALDH+ cells (Fig. 7I, n = 3, $P < 0.01$ for both), and OCSCs markers (Fig. 7J, n = 3, $P < 0.01$ for both) in OCSLCs. Consistently, no difference in cell viability was observed (Supplementary Fig. 8B). Taken together, these results demonstrated that luteolin directly binds to KDM4C and inhibits PPP2CA transcription through suppressing KDM4C-mediated H3K9 demethylation in PPP2CA promoter region.

3.7. Inhibitory effect of luteolin on OC spheroid-derived tumor in vivo

Finally, we investigated the inhibitory effect of luteolin on OC spheroid-derived tumor in vivo. We found that intravenous administration of 100 mg kg^{-1} luteolin (single dose per week) significantly decreased the volume of tumors derived from Caov-3 spheroid cells in xenograft mice and significantly elongated the survival of mice, without obvious weight loss (Fig. 8A and Supplementary Fig. 9A). Moreover, the tumor tissues collected from luteolin-treated mice exhibited decreased the protein levels of PPP2CA, YAP (Fig. 8B). Furthermore, overexpression of KDM4C, PPP2CA and YAP significantly abolished the in vivo inhibitory effect of luteolin on tumor growth (Fig. 8A). These results support that luteolin inhibits OC spheroid-derived tumor by suppressing KDM4C-meidated PPP2CA transcription and YAP stabilization in vivo.

3.8. Luteolin sensitizes chemotherapeutic agents in vivo

The stemness inhibitory effect usually sensitizes the tumor cells to chemotherapeutic agents, we thus investigated whether luteolin sensitizes OC spheroid cells to paclitaxel and carboplatin in vitro and in vivo. As shown in Fig. 9A, Caov-3 and #1 spheroid cells treated with the maximal non-toxic dose of luteolin exhibited significantly lower IC_{50} values of 1.51 and 0.65 nM to paclitaxel, compared to non-treated cells with IC_{50} values of 6.50 and 3.25 nM. The similar results were observed for carboplatin; in combination with luteolin, the carboplatin IC_{50} values reduced by more than 4-fold for both cells (Fig. 9A). Next, the spheroid-derived Caov-3 cells were inoculated into the nude mice to produce the xenograft model. Luteolin alone (0.3 mg kg^{-1} single dose per 1 week), Paclitaxel (15 mg kg^{-1} single dose per 1 week)/carboplatin (40 mg kg^{-1} single dose per 1 week) alone and combined treatment (luteolin + paclitaxel/carboplatin) were administrated intravenously into the mice. As shown in Fig. 9B, there is no obvious difference between vehicle control and luteolin alone groups, suggesting that non-toxic dose of luteolin was administrated. Paclitaxel or carboplatin alone significantly decreased the tumor volume at day 21 compared to vehicle control, while combined treatments leaded to stronger inhibitions compared with paclitaxel or carboplatin alone, without obvious weight loss (Fig. 9B and Supplementary Fig. 9B). Furthermore, combination of luteolin with paclitaxel or carboplatin significantly elongated the survival of xenograft mice compared to paclitaxel or carboplatin alone treatment (Fig. 9B). These results demonstrated that luteolin sensitizes OC spheroid cells to paclitaxel and carboplatin in vitro and in vivo.

Collectively, above results revealed an important mechanism underlying luteolin suppressing OCSCs that luteolin directly binds to KDM4C, blocks KDM4C-mediated histone demethylation of PPP2CA promoter, suppresses PPP2CA transcription and PPP2CA-induced YAP

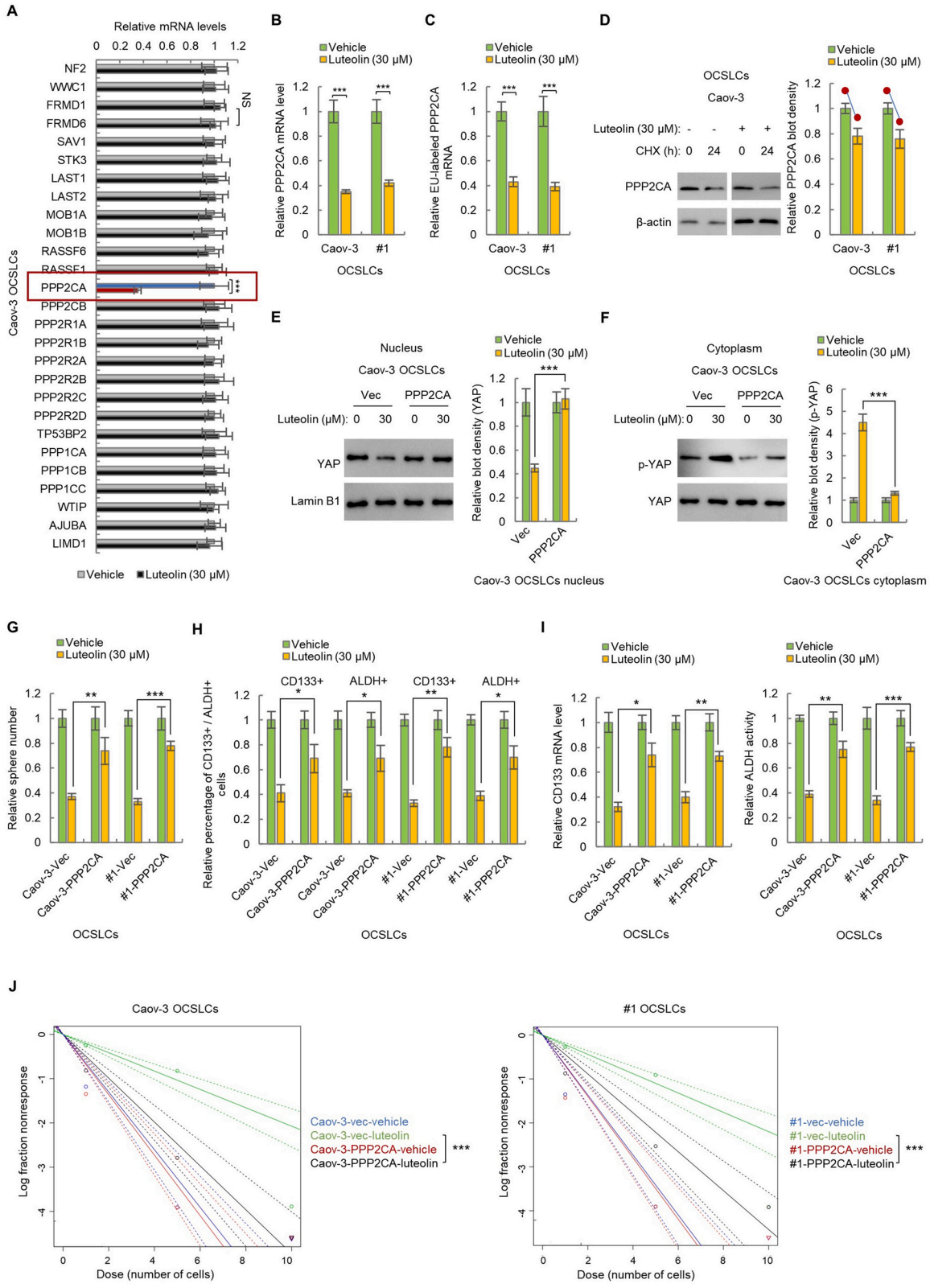

Fig. 6. Luteolin inhibits Hippo/YAP signaling by transcriptional inhibition of PPP2CA. (A) qRT-PCR array analysis of the mRNA levels of the upstream regulators of YAP in indicated cells. (B) qRT-PCR analysis of the mRNA levels of PPP2CA in indicated cells. (C) Nuclear run-on assay analysis of the nascent mRNA levels PPP2CA in indicated cells. (D-F) Western blot analysis of the protein levels of PPP2CA, YAP, and phosphorylated YAP in indicated cells. (G) Sphere-formation assay analysis of sphere-forming capacities of indicated cells. (H) Flow cytometry analysis of the percentages of CD133 + and ALDH+ cells in indicated cells. (I) qRT-PCR and Aldefluor assay analysis of CD133 expression and ALDH activity in indicated cells. (J) In vitro limiting dilution analysis of sphere-initiating capacities of indicated cells. Student's t test and One-way ANOVA analysis, $^{*}P < 0.05$, $^{*}P < 0.01$, $^{*}P < 0.001$.

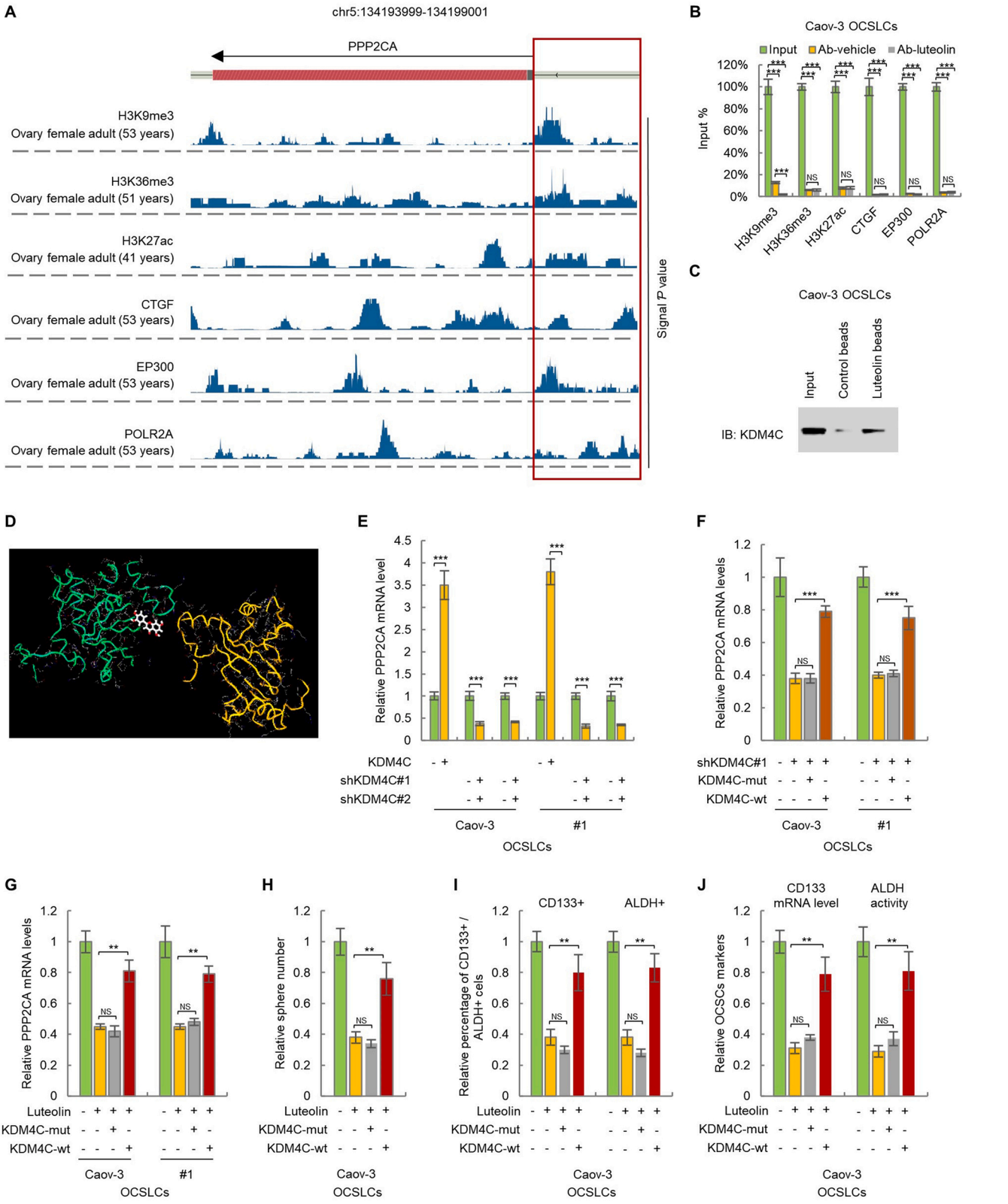

Fig. 7. Luteolin directly binds to KDM4C and inhibits PPP2CA transcription through suppressing KDM4C-mediated H3K9 demethylation in PPP2CA promoter region. (A) ENCODE online software analysis of histone marks and transcription factors engaged to the promoter region of PPP2CA. (B) ChIP-PCR analysis of the effect of luteolin on the abundances of indicated histone marks and transcription factors on PPP2CA promoter. (C) The binding between KDM4C and PPP2CA promoter was analyzed by the binding Assay using luteolin-conjugated beads. (D) The binding between luteolin and KDM4C was predicted by Click Docking online software. (E-G) qRT-PCR analysis of the mRNA levels of PPP2CA in indicated cells. (H) Sphere-formation assay analysis of sphere-forming capacities of indicated cells. (I) Flow cytometry analysis of the percentages of CD133 + and ALDH+ cells in indicated cells. (J) qRT-PCR and Aldefluor assay analysis of CD133 expression and ALDH activity in indicated cells. Student's t test and One-way ANOVA analysis, $^{*}P < 0.05$, $^{*}P < 0.01$, $^{*}P < 0.001$.

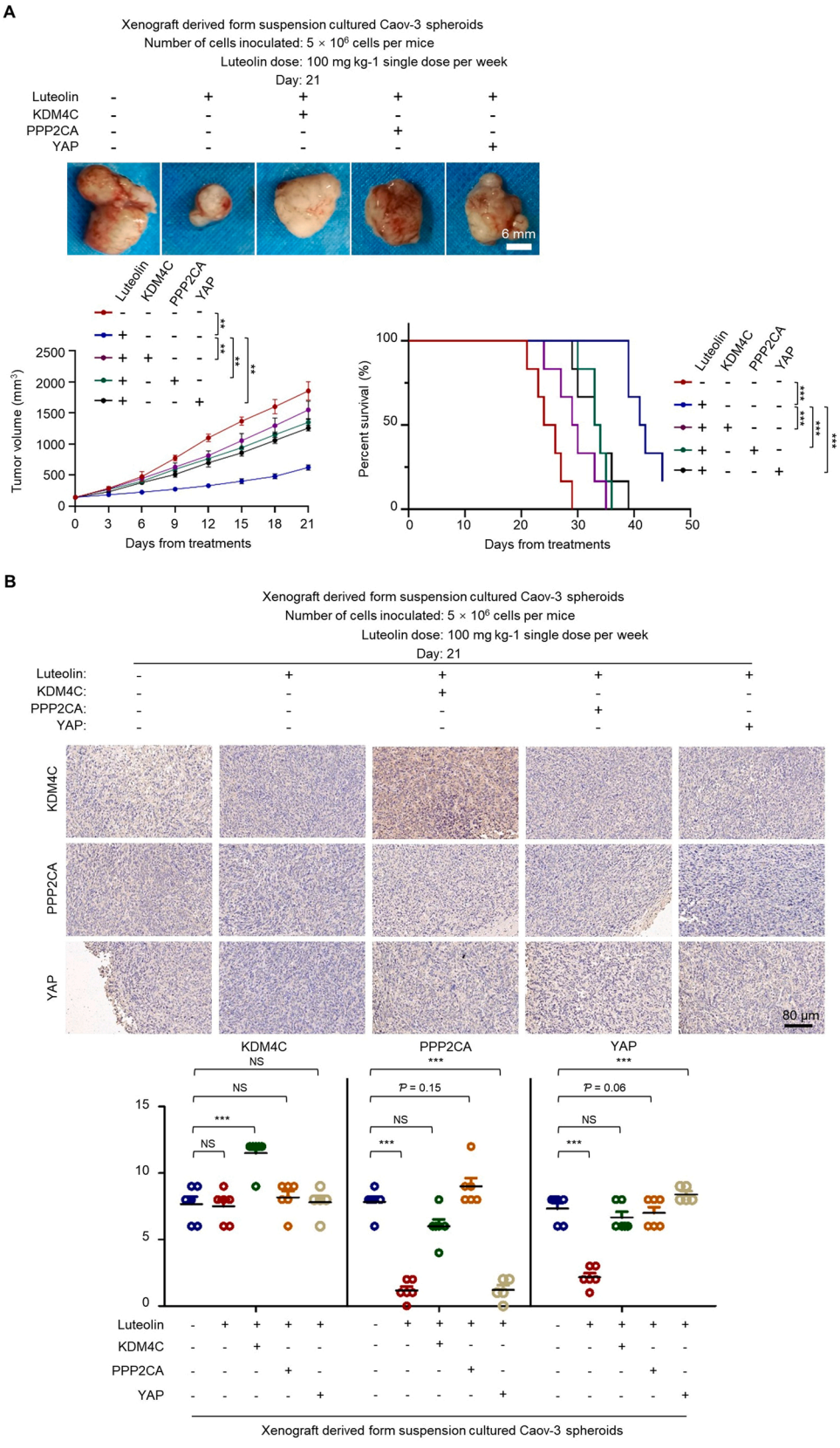

Fig. 8. Inhibitory effect of luteolin on OC spheroid-derived tumor in vivo. (A) Luteolin inhibits OC spheroids-derived tumor growth and elongated the survival in mice bearing OC spheroids-derived tumor by suppressing KDM4C, PPP2CA and YAP. The volume of tumors from mice bearing vector control, KDM4C-, PPP2CA-, YAP-overexpressing OC spheroid cells was recorded. Survival analysis was conducted by Kaplan-meier algorithm. (B) The protein expression of KDM4C, PPP2CA and YAP in indicated samples was analyzed by immunohistochemistry. One-way ANOVA test (n = 3), $*P < 0.05$, $*P < 0.01$, $*P < 0.001$.

dephosphorylation, thereby attenuating YAP activity and the stemness of OCSCs (Fig. 10).

4. Discussion

In this study, we explored KDM4C as a direct target of luteolin that mediates the inhibitory effect of luteolin on the stemness of OCSCs.

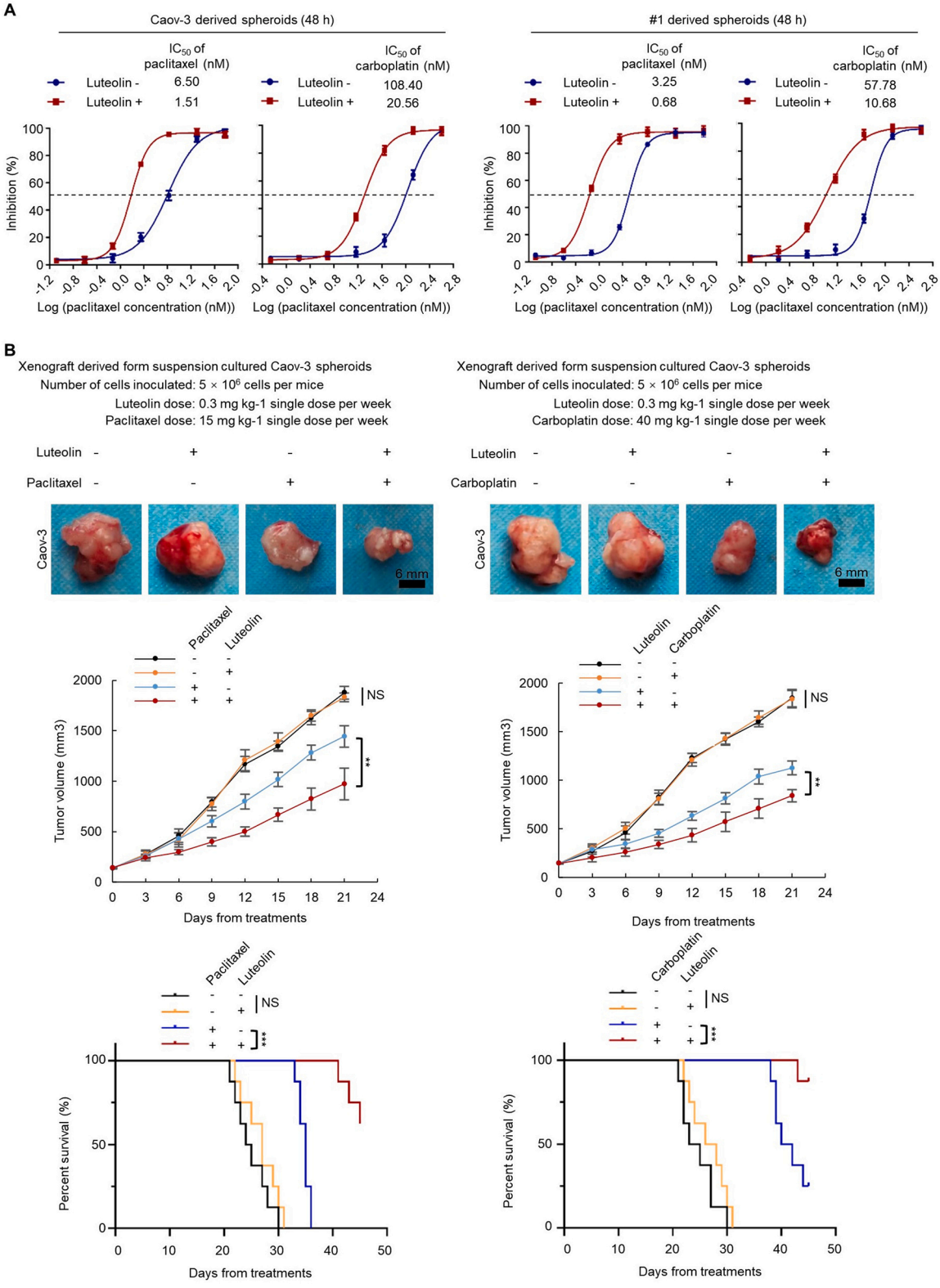

Fig. 9. Luteolin sensitizes chemotherapeutic agents in vivo. (A) Luteolin sensitizes OC spheroid cells to paclitaxel and carboplatin in vitro. The IC_{50} values of paclitaxel and carboplatin in luteolin-treated and non-treated OC spheroid cells were calculated. (B) Luteolin sensitizes OC spheroid cells to paclitaxel and carboplatin in vivo. The tumor growth and the survival of OC spheroids-derived tumor-bearing mice treated with vehicle, luteolin alone, paclitaxel or carboplatin alone, and combination of luteolin and paclitaxel or carboplatin were recorded. One-way ANOVA analysis, $*P < 0.05$, $*P < 0.01$, $*P < 0.001$.

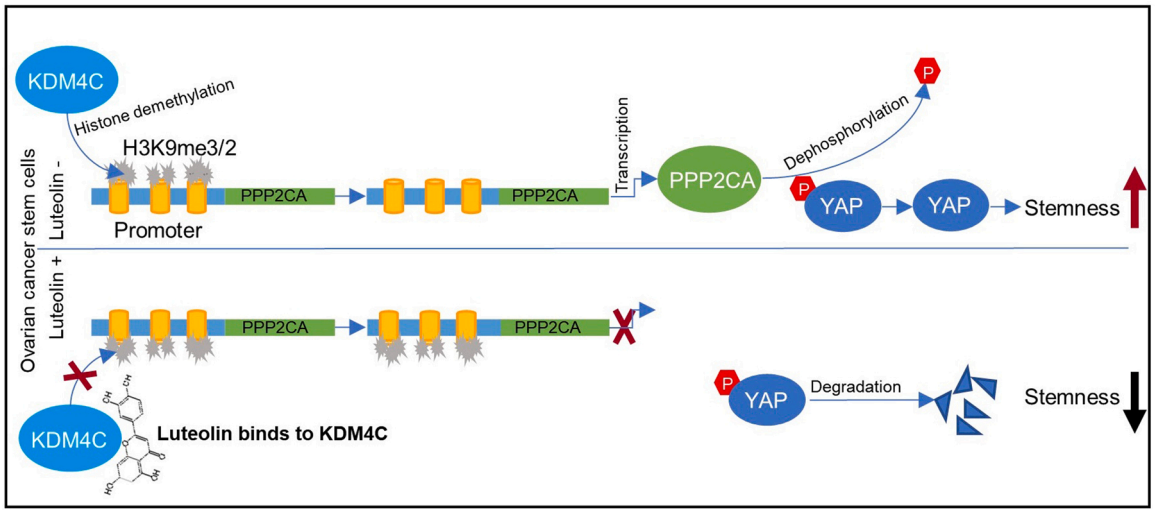

Fig. 10. Schematic representation of mechanism underlying luteolin inhibiting ovarian cancer stemness. Luteolin directly binds to KDM4C, blocks KDM4C-mediated histone demethylation of PPP2CA promoter, inhibits PPP2CA transcription and PPP2CA-induced YAP dephosphorylation, thereby attenuating YAP activity and the stemness of OCSCs.

OCSCs are the main obstacles of OC therapy; OCSCs transformation may happened in different stages of OC initiation and progression and OCSCs are difficult to be removed by both surgery and traditional cytotoxic anti-cancer drugs [37,38]. Thus, revolutionary anti-cancer drugs with relatively low cytotoxicity are urgently needed for long-term use for inhibition of the stemness of OCSCs. Recently, luteolin has been recognized as a promising anti-cancer drug due to its natural origin, better tolerance and relatively low cost; the safety of luteolin have been demonstrated by clinical trials [7,8]. However, although massive studies, the effects of luteolin on OCSCs and the underlying mechanisms were rarely reported. In this study, we demonstrated that maximal non-toxic dose of luteolin inhibits the stemness of OCSCs (Fig. 2 and Supplementary Fig. 2), and the underlying mechanisms that luteolin directly binds to KDM4C and transcriptionally inhibits PPP2CA/YAP signaling was revealed (Figs. 3–7 and Supplementary Figs. 3–8), for the first time. These results thus provide a basis for further development of luteolin as an anti-ovarian cancer drug.

Identification of direct targets of small molecule drugs is difficult. Naoki Kanoh and colleagues developed a photo-cross-linked small-molecule affinity matrix for identifying targets of bioactive small molecules. This technology employs a photogenerated carbene to cross-link small molecules on matrix instead of traditional immobilization strategies in which derivatization of bioactive small molecules is needed; this photo-cross-link-based technology is efficient and loss of bioactivity due to derivatization is effectively avoid [16–20]. Juan Li and colleagues, for the first time, identified that hepatocyte nuclear factor 4α (HNF4α) is the direct target of luteolin [20]. In our study, KDM4C, an oncogene in various types of tumors, was identified as a direct target of luteolin (Fig. 7A-7D). Furthermore, the critical role of KDM4C inhibition for luteolin inhibiting YAP activity was demonstrated (Figs. 7e-7J and Supplementary Fig. 8A and B). These results thus revealed a novel underlying mechanism of anti-cancer effect of luteolin.

Although the oncogenic roles of KDM4C were widely studied, the existence of KDM4C/PPP2CA axis was not reported. To elucidate the mechanism underlying luteolin suppressing the stemness of OCSCs, we investigated the regulator effect of KDM4C on PPP2CA and found that KDM4C promotes PPP2CA transcription through histone demethylation (Fig. 7E and F). Thus, a novel mechanism for KDM4C promoting the stemness of OCSCs was revealed in this study.

The effect of luteolin on KDM4C/PPP2CA/YAP axis is not specifically in OCSCs. In adherent parental cells, the maximal non-toxic dose of luteolin (for parental cells) also inhibited KDM4C/PPP2CA/YAP axis (Supplementary Fig. 10), because KDM4C/PPP2CA/YAP axis is also activated in parental cells. While, compared to traditional therapeutic strategy that attempt to eliminate all cancer cells, an effective therapeutic strategy for cancer should focus on CSCs. Thus, in this study, we focus on the stemness inhibitory effect of luteolin in OCSCs.

5. Conclusion

In summary, our study revealed KDM4C as a novel direct target of luteolin that mediates the stemness inhibitory effect of luteolin in OCSCs, and a novel mechanism that luteolin directly binds to KDM4C and transcriptionally inhibits PPP2CA/YAP axis to attenuate the stemness of OCSCs was explored. Our findings suggest that luteolin is a promising anti-cancer drug candidate for elucidating OCSCs.

Author contributions

Tingyuan Lang designed the study. Tingyuan Lang, Yunzhe Li, and Yunran Hu performed the majority of experiments. Lingling Yang, Jingshu Liu and Chenxi Cui participated the animal experiments. Yunran Hu and Weihong Ge analyzed and interpreted the data from animal experiments. Dongling Zou and Qi Zhou analyzed the results involved in histology and cell behaviors. Yunran Hu, Muyao Yang, and Lei Zhou performed the online analysis. Tingyuan Lang and Weihong Ge supervised the study and wrote, edited and reviewed the manuscript. All the authors have read and approved the final version of the manuscript.

CRediT authorship contribution statement

Tingyuan Lang: Conceptualization, Methodology, Writing – original draft, Writing – review & editing, Supervision. **Yunzhe Li**: Investigation, Resources, Writing – original draft, Writing – review & editing. **Yunran Hu:** Investigation, Resources, Formal analysis. **Lingling Yang**: Investigation, Resources, Visualization. **Jingshu Liu**: Resources. **Chenxi Cui**: Resources, **Dongling Zou**: Formal analysis, **Muyao Yang**: Data curation. **Lei Zhou**: Data curation, **Weihong Ge**: Conceptualization, Writing – review & editing, Supervision. **Qi Zhou**: Conceptualization, Writing – review & editing, Supervision.

Conflict of interest statement

The authors declare that they have no known competing financial

interests or personal relationships that could have appeared to influence the work reported in this paper.

Data Availability

Data will be made available on request.

Acknowledgments

We are grateful to professor Hongbin Ji from Shanghai Institutes for Biological Sciences for providing lentivirus plasmid. This work was supported by Chongqing Science & Technology Commission (CSTB2022NSCQ-MSX1413, cstc2020jxjl130019, cstc2019jscx-msxmX0174). We acknowledge the work of all our colleagues at Chongqing University, Singapore Eye Research Institute, Renji Hospital of Shanghai Jiao Tong University School of Medicine, and Shanghai Fourth People's Hospital of Tongji University School of Medicine.

Appendix A. Supporting information

Supplementary data associated with this article can be found in the online version at doi:10.1016/j.biopha.2023.114350.

References

[1] S. Lheureux, M. Braunstein, A.M. Oza, Epithelial ovarian cancer: evolution of management in the era of precision medicine, CA Cancer J. Clin. 69 (4) (2019) 280–304, https://doi.org/10.3322/caac.21559.
[2] U.A. Matulonis, A.K. Sood, L. Fallowfield, B.E. Howitt, J. Sehouli, B.Y. Karlan, Ovarian cancer, Nat. Rev. Dis. Prim. 2 (2016) 16061, https://doi.org/10.1038/nrdp.2016.61.
[3] C.E. Ford, B. Werner, N.F. Hacker, K. Warton, The untapped potential of ascites in ovarian cancer research and treatment, Br. J. Cancer 123 (1) (2020) 9–16, https://doi.org/10.1038/s41416-020-0875-x.
[4] E. Batlle, H. Clevers, Cancer stem cells revisited, Nat. Med 23 (10) (2017) 1124–1134, https://doi.org/10.1038/nm.4409.
[5] N.K. Lytle, A.G. Barber, T. Reya, Stem cell fate in cancer growth, progression and therapy resistance, Nat. Rev. Cancer 18 (11) (2018) 669–680, https://doi.org/10.1038/s41568-018-0056-x.
[6] M. Matz, M.P. Coleman, M. Sant, M.D. Chirlaque, O. Visser, M. Gore, C. Allemani, the CONCORD Working Group, The histology of ovarian cancer: worldwide distribution and implications for international survival comparisons (CONCORD-2) (2017), Gynecol. Oncol. 144 (2) (2017) 405–413, https://doi.org/10.1016/j.ygyno.2016.10.019.
[7] M. Imran, A. Rauf, T. Abu-Izneid, M. Nadeem, M.A. Shariati, I.A. Khan, A. Imran, I. E. Orhan, M. Rizwan, M. Atif, T.A. Gondal, M.S. Mubarak, Luteolin, a flavonoid, as an anticancer agent: a review, Biomed. Pharm. 112 (2019), 108612, https://doi.org/10.1016/j.biopha.2019.108612.
[8] Â. Bisol, P.S. de Campos, M.L. Lamers, Flavonoids as anticancer therapies: A systematic review of clinical trials, Phytother. Res 34 (3) (2020) 568–582, https://doi.org/10.1002/ptr.6551.
[9] S.F. Nabavi, N. Braidy, O. Gortzi, E. Sobarzo-Sanchez, M. Daglia, K. Skalicka-Woźniak, S.M. Nabavi, Luteolin as an anti-inflammatory and neuroprotective agent: A brief review, Brain Res Bull. 119 (Pt A) (2015) 1–11, https://doi.org/10.1016/j.brainresbull.2015.09.002.
[10] J. Liu, J. Qiu, Z. Zhang, L. Zhou, Y. Li, D. Ding, Y. Zhang, D. Zou, D. Wang, Q. Zhou, T. Lang, SOX4 maintains the stemness of cancer cells via transcriptionally enhancing HDAC1 revealed by comparative proteomics study, Cell Biosci. 11 (1) (2021) 23, https://doi.org/10.1186/s13578-021-00539-y.
[11] L.D. Dunfield, T.G. Shepherd, M.W. Nachtigal, Primary culture and mRNA analysis of human ovarian cells, Biol. Proced. Online 4 (2002) 55–61, https://doi.org/10.1251/bpo34.
[12] Y. Hu, G.K. Smyth, ELDA: extreme limiting dilution analysis for comparing depleted and enriched populations in stem cell and other assays, J. Immunol. Methods 347 (1–2) (2009) 70–78, https://doi.org/10.1016/j.jim.2009.06.008.
[13] A. Turdo, M. Gaggianesi, S. Di Franco, V. Veschi, C. D'Accardo, G. Porcelli, et al., Effective targeting of breast cancer stem cells by combined inhibition of Sam68 and Rad51, Oncogene 41 (15) (2022) 2196–2209, https://doi.org/10.1038/s41388-022-02239-4.
[14] S.T. Smale, Nuclear run-on assay, pdb.prot 5329, Cold Spring Harb. Protoc. 11 (2009), https://doi.org/10.1101/pdb.prot5329.
[15] J.A. Dahl, P. Collas, A rapid micro chromatin immunoprecipitation assay (microChIP), Nat. Protoc. 3 (6) (2008) 1032–1045, https://doi.org/10.1038/nprot.2008.68.
[16] N. Kanoh, K. Honda, S. Simizu, M. Muroi, H. Osada, Photo-cross-linked small-molecule affinity matrix for facilitating forward and reverse chemical genetics, Angew. Chem. Int Ed. Engl. 44 (23) (2005) 3559–3562, https://doi.org/10.1002/anie.200462370.
[17] N. Kanoh, S. Kumashiro, S. Simizu, Y. Kondoh, S. Hatakeyama, H. Tashiro, H. Osada, Immobilization of natural products on glass slides by using a photoaffinity reaction and the detection of protein-small-molecule interactions, Angew. Chem. Int Ed. Engl. 42 (45) (2003) 5584–5587, https://doi.org/10.1002/anie.200352164.
[18] P.D. Beer, J. Cadman, J.M. Lloris, R. Martínez-Máñez, J. Soto, T. Pardo, C. Vera, M. Marcos, Anion interaction with ferrocene-functionalised cyclic and open-chain polyaza and aza-oxa cycloalkanes, J. Chem. Soc. Dalton Trans. 11 (2000) 1805–1812, https://doi.org/10.1039/b000079p.
[19] M. Kawatani, H. Okumura, K. Honda, N. Kanoh, M. Muro, N. Dohmae, M. Takami, M. Kitagawa, Y. Futamura, M. Imoto, H. Osada, The identification of an osteoclastogenesis inhibitor through the inhibition of glyoxalase I, Proc. Natl. Acad. Sci. USA 105 (33) (2008) 11691–11696, https://doi.org/10.1073/pnas.0712239105.
[20] J. Li, J. Inoue, J.M. Choi, S. Nakamura, Z. Yan, S. Fushinobu, H. Kamada, H. Kato, T. Hashidume, M. Shimizu, R. Sato, Identification of the flavonoid luteolin as a repressor of the transcription factor hepatocyte nuclear factor 4α, J. Biol. Chem. 290 (39) (2015) 24021–24035, https://doi.org/10.1074/jbc.M115.645200.
[21] M.D. Curley, V.A. Therrien, C.L. Cummings, P.A. Sergent, C.R. Koulouris, A. M. Friel, et al., CD133 expression defines a tumor initiating cell population in primary human ovarian cancer, Stem Cells (Dayt., Ohio) 27 (12) (2009) 2875–2883, https://doi.org/10.1002/stem.236.
[22] S. Condello, C. A.Morgan, S. Nagdas, L. Cao, J. Turek, T.D. Hurley, D. Matei, β-Catenin-regulated ALDH1A1 is a target in ovarian cancer spheroids, Oncogene 34 (18) (2015) 2297–2308, https://doi.org/10.1038/onc.2014.178.
[23] Y. Zhang, Y. Wang, G. Zhao, E.J. Tanner, M. Adli, D. Matei, FOXK2 promotes ovarian cancer stemness by regulating the unfolded protein response pathway, J. Clin. Investig. 132 (10) (2022), e151591, https://doi.org/10.1172/JCI151591.
[24] S. Al Hayek, A. Alsawadi, Z. Kambris, J.P. Boquete, J. Bohère, C. Immarigeon, et al., Steroid-dependent switch of OvoL/Shavenbaby controls self-renewal versus differentiation of intestinal stem cells, EMBO J. 40 (4) (2021), e104347, https://doi.org/10.15252/embj.2019104347.
[25] M. Ognibene, A. Pezzolo, Roniciclib down-regulates stemness and inhibits cell growth by inducing nucleolar stress in neuroblastoma, Sci. Rep. 10 (1) (2020) 12902, https://doi.org/10.1038/s41598-020-69499-6.
[26] T.T. Wang, S.K. Wang, G.L. Huang, G.J. Sun, Luteolin induced-growth inhibition and apoptosis of human esophageal squamous carcinoma cell line Eca109 cells in vitro, APJCP 13 (11) (2012) 5455–5461, https://doi.org/10.7314/apjcp.2012.13.11.5455.
[27] Y.S. Kim, S.H. Kim, J. Shin, A. Harikishore, J.K. Lim, Y. Jung, et al., Luteolin suppresses cancer cell proliferation by targeting vaccinia-related kinase 1, PloS One 9 (10) (2014), e109655, https://doi.org/10.1371/journal.pone.0109655.
[28] K. Han, T. Lang, Z. Zhang, Y. Zhang, Y. Sun, Z. Shen, R.W. Beuerman, L. Zhou, D. Min, Luteolin attenuates Wnt signaling via upregulation of FZD6 to suppress prostate cancer stemness revealed by comparative proteomics, Sci. Rep. 8 (1) (2018) 8537, https://doi.org/10.1038/s41598-018-26761-2.
[29] Y. Liu, T. Lang, B. Jin, F. Chen, Y. Zhang, R.W. Beuerman, L. Zhou, Z. Zhang, Luteolin inhibits colorectal cancer cell epithelial-to-mesenchymal transition by suppressing CREB1 expression revealed by comparative proteomics study, J. Proteom. 161 (2017) 1–10, https://doi.org/10.1016/j.jprot.2017.04.005.
[30] H.M. Zhou, J.G. Zhang, X. Zhang, Q. Li, Targeting cancer stem cells for reversing therapy resistance: mechanism, signaling, and prospective agents, Signal Transduct. Target. Ther. 6 (1) (2021) 62, https://doi.org/10.1038/s41392-020-00430-1.
[31] T. Shibue, R.A. Weinberg, EMT, CSCs, and drug resistance: the mechanistic link and clinical implications, Nat. Rev., Clin. Oncol. 14 (10) (2017) 611–629, https://doi.org/10.1038/nrclinonc.2017.44.
[32] I.G. Kim, J.H. Lee, S.Y. Kim, C.K. Heo, R.K. Kim, E.W. Cho, Targeting therapy-resistant lung cancer stem cells via disruption of the AKT/TSPYL5/PTEN positive-feedback loop, Commun. Biol. 4 (1) (2021) 778, https://doi.org/10.1038/s42003-021-02303-x.
[33] A. Singh, J. Settleman, EMT, cancer stem cells and drug resistance: an emerging axis of evil in the war on cancer, Oncogene 29 (34) (2010) 4741–4751, https://doi.org/10.1038/onc.2010.215.
[34] L. Yang, P. Shi, G. Zhao, J. Xu, W. Peng, J. Zhang, et al., Targeting cancer stem cell pathways for cancer therapy, Signal Transduct. Target. Ther. 5 (1) (2020) 8, https://doi.org/10.1038/s41392-020-0110-5.
[35] F. Zanconato, M. Cordenons, S. Piccolo, YAP and TAZ: a signalling hub of the tumour microenvironment, Nat. Rev. Cancer 19 (8) (2019) 454–464, https://doi.org/10.1038/s41568-019-0168-y.
[36] ENCODE Project Consortium, An integrated encyclopedia of DNA elements in the human genome, Nature 489 (7414) (2012) 57–74, https://doi.org/10.1038/nature11247.
[37] M.Q. Gao, Y.P. Choi, S. Kang, J.H. Youn, N.H. Cho, CD24+ cells from hierarchically organized ovarian cancer are enriched in cancer stem cells, Oncogene 29 (18) (2010) 2672–2680, https://doi.org/10.1038/onc.2010.35.
[38] M. Varas-Godoy, G. Rice, S.E. Illanes, The crosstalk between ovarian cancer stem cell niche and the tumor microenvironment, Stem Cells Int. (2017) 5263974, https://doi.org/10.1155/2017/5263974.